

This is a preprint of an article whose final and definitive form has been published in the International Journal of Green Energy, Vol. 8, 2011, 429–473 (copyright Taylor & Francis) and is available online at <http://www.tandfonline.com/doi/abs/10.1080/15435075.2011.576287>.

Thermally Reversible Hydrino Catalyst Systems as a New Power Source

R. L. Mills¹, G. Zhao, K. Akhtar, Z. Chang, J. He, X. Hu, G. Wu, J. Lotoski, G. Chu

BlackLight Power, Inc., 493 Old Trenton Road, Cranbury, NJ 08512

ABSTRACT

Energy balances were measured for representative thermally regenerative reactions of four classes of hydrino catalyst systems, each capable of resonantly accepting $m \times 27.2$ eV from H to form $H(1/p)$, Rydberg states of atomic hydrogen called “hydrino atoms” wherein $n=1/2, 1/3, 1/4, \dots, 1/p$ ($p \leq 137$ is an integer) replaces the well-known parameter n =integer in the Rydberg equation for hydrogen excited states. Specifically, hydride-halide exchange reactions were tested wherein K and NaH served as catalysts since they form K^{3+} and Na^{2+} ions by absorbing 3×27.2 eV and 2×27.2 eV, respectively. Typical parameters measured by absolute water-flow calorimetry were 2-5 times energy gain relative to regeneration chemistry and 7 Wcm^{-3} . The predicted molecular hydrino and hydrino hydride products $H_2(1/4)$ and $H^-(1/4)$ corresponding to 50 MJ/mole H_2 consumed were confirmed by the solution ^1H NMR peak at 1.2 ppm and XPS peak at 11 eV, respectively.

Keywords: hydrino catalyst reactions, thermal regeneration, molecular hydrino, hydrino hydride ion, calorimetry, NMR spectroscopy and XPS

¹ Corresponding author: rmills@blacklightpower.com; phone: 1-609-490-1090; fax: 1-609-490-1066

1. Introduction

1.1. Theory of Catalytic Lower-Energy Hydrogen Electronic Transitions and Supporting Data

Classical physics (CP) gives closed-form solutions of the hydrogen atom, the hydride ion, the hydrogen molecular ion, and the hydrogen molecule and predicts corresponding species having fractional principal quantum numbers [1–13]. The nonradiative state of atomic hydrogen, which is historically called the “ground state” forms the basis of the boundary condition of CP to solve the bound electron. CP predicts a reaction involving a resonant, nonradiative energy transfer from otherwise stable atomic hydrogen to a catalyst capable of accepting the energy to form hydrogen in lower-energy states than previously thought possible. Specifically, CP predicts that atomic hydrogen may undergo a catalytic reaction with certain atoms, excimers, ions, and diatomic hydrides which provide a reaction with a net enthalpy of an integer multiple of the potential energy of atomic hydrogen, $E_n = 27.2 \text{ eV}$ where E_n is one Hartree. Specific species (e.g. He^+ , Ar^+ , Sr^+ , K , Li , HCl , and NaH) identifiable on the basis of their known electron energy levels are required to be present with atomic hydrogen to catalyze the process. The reaction involves a nonradiative energy transfer of an integer multiple of 27.2 eV from atomic hydrogen to the catalyst followed by $q \times 13.6 \text{ eV}$ continuum emission or $q \times 13.6 \text{ eV}$ (q is an integer matching the sum of eq. (7)) transfer to another H to form extraordinarily hot, excited-state H and a hydrogen atom that is lower in energy than unreacted atomic hydrogen that corresponds to a fractional principal quantum number. That is, in the formula for the principal energy levels of the hydrogen atom:

$$E_n = -\frac{e^2}{n^2 8\pi\epsilon_0 a_H} = -\frac{13.598 \text{ eV}}{n^2} \quad (1)$$

$$n = 1, 2, 3, \dots \quad (2)$$

where a_H is the Bohr radius for the hydrogen atom (52.947 pm), e is the magnitude of the charge of the electron, and ε_0 is the vacuum permittivity, fractional quantum numbers:

$$n = 1, \frac{1}{2}, \frac{1}{3}, \frac{1}{4}, \dots, \frac{1}{p}; \quad p \leq 137 \text{ is an integer} \quad (3)$$

that replaces the well known parameter $n = \text{integer}$ in the Rydberg equation for hydrogen excited states. Then, a hydrino atom also comprises an electron, a proton, and a photon. However, the electric field of the latter increases the binding corresponding to desorption of energy rather than decreasing the central field with the absorption of energy as in an excited state, and the resultant photon-electron interaction of the hydrino is stable rather than radiative. The Maxwellian solutions to both excited and hydrino states are given in Ref. [1].

The $n = 1$ state of hydrogen and the $n = 1/\text{integer}$ states of hydrogen are nonradiative, but a transition between two nonradiative states, say $n = 1$ to $n = 1/2$, is possible via a nonradiative energy transfer. Hydrogen is a special case of the stable states given by Eqs. (1) and (3) wherein the corresponding radius of the hydrogen or hydrino atom is given by

$$r = \frac{a_H}{p}, \quad (4)$$

where $p = 1, 2, 3, \dots$. In order to conserve energy, energy must be transferred from the hydrogen atom to the catalyst in units of

$$m \times 27.2 \text{ eV}, \quad m = 1, 2, 3, 4, \dots \quad (5)$$

and the radius transitions to $a_H/(m + p)$. The catalyst reactions involve two steps of energy release [1, 14, 15]: a nonradiative energy transfer to the catalyst followed by additional energy

release as the radius decreases to the corresponding stable final state. Thus, the general reaction is given by

$$m \cdot 27.2 \text{ eV} + \text{Cat}^{q+} + \text{H} \left[\frac{a_{\text{H}}}{p} \right] \rightarrow \text{Cat}^{(q+r)+} + re^{-} + \text{H}^* \left[\frac{a_{\text{H}}}{(m+p)} \right] + m \cdot 27.2 \text{ eV} \quad (6)$$

$$\text{H}^* \left[\frac{a_{\text{H}}}{(m+p)} \right] \rightarrow \text{H} \left[\frac{a_{\text{H}}}{(m+p)} \right] + [(m+p)^2 - p^2] \cdot 13.6 \text{ eV} - m \cdot 13.6 \text{ eV} \quad (7)$$

$$\text{Cat}^{(q+r)+} + re^{-} \rightarrow \text{Cat}^{q+} + m \cdot 27.2 \text{ eV} \quad (8)$$

And, the overall reaction is

$$\text{H} \left[\frac{a_{\text{H}}}{p} \right] \rightarrow \text{H} \left[\frac{a_{\text{H}}}{(m+p)} \right] + [(m+p)^2 - p^2] \cdot 13.6 \text{ eV} \quad (9)$$

q , r , m , and p are integers. $\text{H}^* \left[\frac{a_{\text{H}}}{(m+p)} \right]$ has the radius of the hydrogen atom

(corresponding to $p = 1$) and a central field equivalent to $(m+p)$ times that of a proton, and

$\text{H} \left[\frac{a_{\text{H}}}{(m+p)} \right]$ is the corresponding stable state with the radius of $1/(m+p)$ that of H. As the

electron undergoes radial acceleration from the radius of the hydrogen atom to a radius of

$(m+p)$ this distance, energy is released as characteristic light emission or as third-body kinetic

energy. The emission may be in the form of an extreme-ultraviolet continuum radiation having

an edge at $[(m+p)^2 - p^2 - 2m] \cdot 13.6 \text{ eV}$ or $91.2/[(m+p)^2 - p^2 - 2m] \text{ nm}$ and extending to

longer wavelengths. In addition to radiation, a resonant kinetic energy transfer to form fast H

may occur. Subsequent excitation of these fast H ($n = 1$) atoms by collisions with the

background H_2 followed by emission of the corresponding H ($n = 3$) fast atoms gives rise to

broadened Balmer α emission. Extraordinary ($>100 \text{ eV}$) Balmer α line broadening is observed

consistent with predictions [14–28].

As given in Chp. 5 of Ref [1], and Refs. [14–17], hydrogen atoms

H($1/p$) $p = 1, 2, 3, \dots, 137$ can undergo further transitions to lower-energy states given by Eqs. (1) and (3) wherein the transition of one atom is catalyzed by a second that resonantly and nonradiatively accepts $m \times 27.2$ eV with a concomitant opposite change in its potential energy. The overall general equation for the transition of H ($1/p$) to H ($1/(m+p)$) induced by a resonance transfer of $m \times 27.2$ eV to H($1/p'$) is represented by

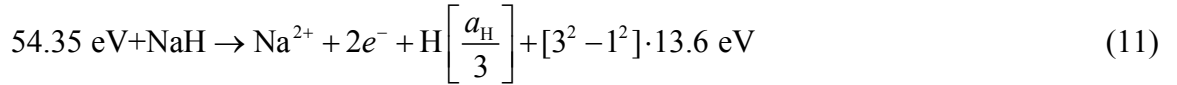
$$H(1/p') + H(1/p) \rightarrow H + H(1/(m+p)) + [2pm + m^2 - p'^2 + 1] \cdot 13.6 \text{ eV} \quad (10)$$

Hydrogen atoms may serve as a catalyst wherein $m = 1$, $m = 2$, and $m = 3$ for one, two, and three atoms, respectively, acting as a catalyst for another. The rate for the two-atom-catalyst, 2H, may be high when extraordinarily fast H as reported previously [14, 17–28] collides with a molecule to form the 2H wherein two atoms resonantly and nonradiatively accept 54.4 eV from a third hydrogen atom of the collision partners. By the same mechanism, the collision of two hot H₂ provide 3H to serve as a catalyst of 3×27.2 eV for the fourth. The EUV continua at 22.8 nm and 10.1 nm, extraordinary (>50 eV) Balmer α line broadening, highly excited H states, and the product gas H₂($1/4$) were observed as predicted [14, 15].

Thus, a catalyst provides a net positive enthalpy of reaction of $m \times 27.2$ eV (i.e. it resonantly accepts the nonradiative energy transfer from hydrogen atoms and releases the energy to the surroundings to affect electronic transitions to fractional quantum energy levels). K can serve as a catalyst since the ionization of K to K³⁺ is about 81.6 eV (3×27.2 eV). As a consequence of the nonradiative energy transfer, the hydrogen atom becomes unstable and emits further energy until it achieves a lower-energy nonradiative state having a principal energy level given by Eqs. (1) and (3). Thus, the catalysis releases energy from the hydrogen atom with a commensurate decrease in size of the hydrogen atom, $r_n = na_H$ where n is given by Eq. (3). For example, the catalysis of H ($n = 1$) to H($n = 1/4$) releases 204 eV, and the hydrogen radius

decreases from a_H to $\frac{1}{4}a_H$.

A compound comprising hydrogen such as MH , where M is an element other than hydrogen, serves as a source of hydrogen and a source of catalyst. A catalytic reaction is provided by the breakage of the $M-H$ bond plus the ionization of t electrons from the atom M each to a continuum energy level such that the sum of the bond energy and ionization energies of the t electrons is approximately $m \times 27.2$ eV, where m is an integer. One such catalytic system involves sodium hydride. The bond energy of NaH is 1.9245 eV [29], and the first and second ionization energies of Na are 5.13908 eV and 47.2864 eV, respectively [30]. Based on these energies NaH molecule can serve as a catalyst and H source, since the bond energy of NaH plus the double ionization ($t = 2$) of Na to Na^{2+} is 54.35 eV (2×27.2 eV). The concerted catalyst reactions are given by



And, the overall reaction is



With $m = 2$, the product of catalyst NaH is H (1/3) that reacts rapidly to form H (1/4), then molecular hydrino, $H_2(1/4)$, as a preferred state. Specifically, in the case of a high hydrogen atom concentration, the further transition given by Eq. (10) of H (1/3) ($p = 3$) to H (1/4) ($p + m = 4$) with H as the catalyst ($p' = 1$; $m = 1$) can be fast:



The corresponding molecular hydrino $H_2(1/4)$ and hydrino hydride ion $H^-(1/4)$ are preferred final products [14–18, 31–35] consistent with observation since the $p = 1$ quantum state has a multipolarity greater than that of a quadrupole giving $H(1/4)$ a long theoretical lifetime [17] for further catalysis.

The catalyst product, $H(1/p)$, may also react with an electron to form a hydrino hydride ion $H^-(1/p)$, or two $H(1/p)$ may react to form the corresponding molecular hydrino $H_2(1/p)$. Specifically, the catalyst product, $H(1/p)$, may also react with an electron to form a novel hydride ion $H^-(1/p)$ with a binding energy E_B [1, 16–18, 31–35]:

$$E_B = \frac{\hbar^2 \sqrt{s(s+1)}}{8\mu_e a_0^2 \left[\frac{1 + \sqrt{s(s+1)}}{p} \right]^2} - \frac{\pi\mu_0 e^2 \hbar^2}{m_e^2} \left(\frac{1}{a_H^3} + \frac{2^2}{a_0^3 \left[\frac{1 + \sqrt{s(s+1)}}{p} \right]^3} \right) \quad (15)$$

where $p = \text{integer} > 1$, $s = 1/2$, \hbar is Planck's constant bar, μ_0 is the permeability of vacuum, m_e is the mass of the electron, μ_e is the reduced electron mass given by

$\mu_e = m_e m_p / \left[\left(m_e / \sqrt{3/4} \right) + m_p \right]$ where m_p is the mass of the proton, a_0 is the Bohr radius, and

the ionic radius is $r_1 = \frac{a_0}{p} \left(1 + \sqrt{s(s+1)} \right)$. From Eq. (15), the calculated ionization energy of the hydride ion is 0.75418 eV, and the experimental value given by Lykke [36] is $6082.99 \pm 0.15 \text{ cm}^{-1}$ (0.75418 eV).

Upfield-shifted NMR peaks are direct evidence of the existence of lower-energy state hydrogen with a reduced radius relative to ordinary hydride ion and having an increase in diamagnetic shielding of the proton. The shift is given by the sum of that of an ordinary hydride ion H^- and a component due to the lower -energy state [1, 18]:

$$\frac{\Delta B_T}{B} = -\mu_0 \frac{e^2}{12m_e a_0 (1 + \sqrt{s(s+1)})} (1 + \alpha 2\pi p) = -(29.9 + 1.37p) \text{ ppm} \quad (16)$$

where for H^- $p = 0$ and $p = \text{integer} > 1$ for $H^-(1/p)$ and α is the fine structure constant.

The calculated and experimental parameters of H_2 , D_2 , H_2^+ , and D_2^+ from Ref. [1, 7] are given in Table 1. $H(1/p)$ may react with a proton and two $H(1/p)$ may react to form $H_2(1/p)^+$ and $H_2(1/p)$, respectively. The hydrogen molecular ion and molecular charge and current density functions, bond distances, and energies were solved previously [1, 7].

The NMR of catalysis-product gas provides a definitive test of the theoretically predicted chemical shift of $H_2(1/4)$. In general, the 1H NMR resonance of $H_2(1/p)$ is predicted to be upfield from that of H_2 due to the fractional radius in elliptic coordinates [1, 7] wherein the electrons are significantly closer to the nuclei. The predicted shift, $\frac{\Delta B_T}{B}$, for $H_2(1/p)$ derived previously [1, 7] is given by the sum of that of H_2 and a term that depends on $p = \text{integer} > 1$ for $H_2(1/p)$:

$$\frac{\Delta B_T}{B} = -\mu_0 \left(4 - \sqrt{2} \ln \frac{\sqrt{2} + 1}{\sqrt{2} - 1} \right) \frac{e^2}{36a_0 m_e} (1 + \pi \alpha p) \quad (17)$$

$$\frac{\Delta B_T}{B} = -(28.01 + 0.64p) \text{ ppm} \quad (18)$$

where for H_2 $p = 0$. The experimental absolute H_2 gas-phase resonance shift of -28.0 ppm [37–40] is in excellent agreement with the predicted absolute gas-phase shift of -28.01 ppm (Eq. (18)).

The data from a broad spectrum of investigational techniques strongly and consistently indicates that hydrogen can exist in lower-energy states than previously thought possible and support the existence of these states called hydrino, for “small hydrogen,” and the

corresponding hydride ions and molecular hydrino. Some of these prior related studies supporting the possibility of a novel reaction of atomic hydrogen, which produces hydrogen in fractional quantum states that are at lower energies than the traditional “ground” ($n = 1$) state, include extreme ultraviolet (EUV) spectroscopy, characteristic emission from catalysts and the hydride ion products, lower-energy hydrogen emission, chemically-formed plasmas, Balmer α line broadening, population inversion of H lines, elevated electron temperature, anomalous plasma afterglow duration, power generation, and analysis of novel chemical compounds [14–28, 31–35, 41–52].

Catalyst systems reported previously [16] comprised (i) a catalyst or source of catalyst and a source of hydrogen from the group of LiH, KH, and NaH, (ii) an oxidant from the group of NiBr₂, MnI₂, AgCl, EuBr₂, SF₆, S, CF₄, NF₃, LiNO₃, M₂S₂O₈ with Ag, and P₂O₅, (iii) a reductant from the group of Mg powder, or MgH₂, Al powder, or aluminum nano-powder (Al NP), Sr, and Ca, and (iv) a support from the group of AC, TiC, and YC₂. The typical metallic form of Li and K were converted to the atomic form and the ionic form of NaH was converted to the molecular form by using support such as an activated carbon (AC) having a surface area of 900 m²/g to disperse Li and K atoms and NaH molecules, respectively. The reaction step (Eq. (6)) of a nonradiative energy transfer of an integer multiple of 27.2 eV from atomic hydrogen to the catalyst results in ionized catalyst and free electrons that causes the reaction to rapidly cease due to charge accumulation. The support also acted as a conductive electron acceptor of electrons released from the catalyst reaction to form hydrinos. Each reaction mixture further comprised an oxidant to serve as scavenger of electrons from the conductive support and a final electron-acceptor reactant as well as a weak reductant to assist the oxidant’s function. In some cases, the concerted electron-acceptor (oxidation) reaction was also very exothermic to heat the reactants

and enhance the rates to produce power or hydrino compounds. The energy balances of the heterogeneous catalyst systems were measured by water-flow calorimetry, and the hydrino products were characterized by ^1H Nuclear Magnetic Resonance (NMR), Time-of-Flight Secondary Mass Spectroscopy (ToF-SIMS), and X-ray photoelectron spectroscopy (XPS). The heat was also recorded on a 10-fold scale-up reaction. The measured power and energy gain from these heterogeneous catalyst systems were up to $10 \text{ W} / \text{cm}^3_{(\text{reactant volume})}$ and a factor of over six times the maximum theoretical, respectively. The reaction scaled linearly to 580 kJ that developed a power of about 30 kW. Solution ^1H NMR on samples extracted from the reaction products in DMF-d7 showed the predicted $\text{H}_2(1/4)$ and $\text{H}^-(1/4)$ at 1.2 ppm and -3.8 ppm, respectively. ToF-SIMS showed sodium hydrino hydride peaks such as NaH_x , peaks with NaH catalyst, and the predicted 11 eV binding energy of $\text{H}^-(1/4)$ was observed by XPS. In this paper, the findings on the reaction mechanism of hydrino formation were applied to the development of a thermally reversible chemistry as a new power source.

1.2. Thermally Reversible Hydrino Catalyst Systems

Four classes of reactions were developed that form hydrinos using a thermally reversible reaction mixture of a catalyst or source of catalyst and a source of hydrogen (KH or NaH), a high-surface-area conductive support (TiC, TiCN, Ti_3SiC_2 , WC, YC_2 , Pd/C, carbon black (CB), and LiCl reduced to Li), and optionally a reductant (Mg, Ca, Li). Additionally, two systems comprised an alkaline earth or alkali halide oxidant, or the carbon support comprised the oxidant. These reactants (Table 2) form predictable products based on the corresponding maximum heat release E_{mt} calculable from the known enthalpies of the reactants and products as given in Table

3.

The first type of reaction to propagate hydride formation was an oxidation-reduction reaction involving hydride-halide exchange between NaH or KH and an alkaline earth halide. In a representative reaction, the exchange is



where $M = \text{Mg, Ca, Sr, Ba}$; $X = \text{F, Cl, Br, I}$. The corresponding reaction mixtures such as $\text{KH} + \text{Mg} + \text{TiC} + \text{MX}_2$ are similar to those reported previously [16] with the primary difference being that the oxidant MX_2 replaced a member of the group of $\text{NiBr}_2, \text{MnI}_2, \text{AgCl}, \text{EuBr}_2, \text{SF}_6, \text{S}, \text{CF}_4, \text{NF}_3, \text{LiNO}_3, \text{K}_2\text{S}_2\text{O}_8$ with Ag , and P_2O_5 . The latter systems produced high power, energy output and energy gain, but with exception of EuBr_2 and possibly MnI_2 , the systems could not be conveniently thermally regenerated. The transition to alkaline earth halides solved this problem while achieving similar power production. The forward reaction was spontaneous to form NaX or KX and MH_2 , but it was observed that the equilibrium could be shifted from predominantly the products to the reverse direction by dynamically removing the volatile reverse-reaction product, the alkali metal. Alkaline earth metal hydrides MH_2 decompose at elevated temperature under vacuum [53], and the reaction of the metal M with KX was shown to occur with favorable kinetics. Specifically, the alkaline earth halides were formed by the reaction of the corresponding alkaline earth metal and potassium halide at elevated temperature (650–800 °C) as the potassium metal was evaporated and separately condensed. The reaction conditions and results are shown in Table 4.

An alkali metal halide may also serve as the oxidant. Since the catalyst metal is also an alkali metal the regeneration of the reactants from alkali metal hydride and halide products would give rise to metals competing in evaporation and halide reactions with mixtures of both expected. However, Li has unique characteristics that enable selectivity of the regeneration

reactions. LiH is stable to 900 °C [54] and melts at 688.7 °C [55]; thus, lithium halides such as LiCl and LiBr may serve as the oxidant or halide of a hydride-halide exchange reaction wherein another catalyst metal such as K or Na is preferentially evaporated during regeneration as LiH reacts to form the initial lithium halide. The reaction mixture comprised the source of catalyst and hydrogen NaH or KH, the reductant alkaline earth metal Mg powder, a support such as TiC, and the oxidant, alkali halides LiCl or LiBr. The products were sodium or potassium halide and lithium hydride. Then, exemplary power producing hydrino reaction and regeneration reaction are



and



respectively, wherein X is Cl or Br since they gave the best results in this system. K is preferentially evaporated due to the high volatility of K and the relative instability of KH compared to LiH. The metal K may be separately hydrided and returned to the reaction mixture to regenerate it. Alternatively, Li replaces LiH in the regeneration reaction since it has a much lower vapor pressure than K. For example at 722 °C, the vapor pressure of Li is 100 Pa; whereas, at a similar temperature, 756 °C, the vapor pressure of K is 100 kPa [56]. Then, K can be selectively evaporated during a regeneration reaction between KX and Li in Eq. (21).

In addition to metal halides, carbon can serve the role of the oxidant. Thus, the second type of reaction to propagate hydrino formation was an oxidation-reduction reaction wherein the carbon support served as the oxidant during the reaction with KH to form the intercalation compound KHC_x [57–59]:

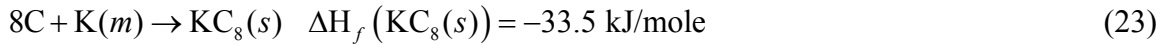


Graphite intercalation compounds are formed by the insertion of atomic or molecular layers of a different chemical species called the intercalant between layers in a graphite host material.

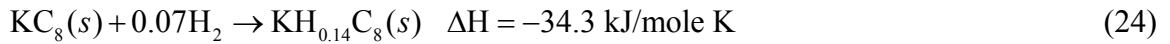
Alkali metal-graphite has a large increase in electrical conductivity from a charge transfer from the intercalate layer where the carriers have a low mobility to the graphite layers where the mobility is high. In an exemplary reaction, the intercalation compound may be KC_x wherein x may be 8, 10, 24, 36, 48, 60 [58, 59]. In this case, the oxidation states of the species are $K^+C_x^-$.

Potassium graphite can further bond H in the inter-graphitic plane [57] to form KHC_x . Since the bonding is weak, the intercalation compound may be thermally regenerated to the metal and carbon.

Sangster gives the heat of formation of $KC_8(s)$ [59]:



Enoki [57] gives the energy of H reacting with KC_8 wherein the most exothermic reaction per K is at the lowest H composition of 0.14 H per K:



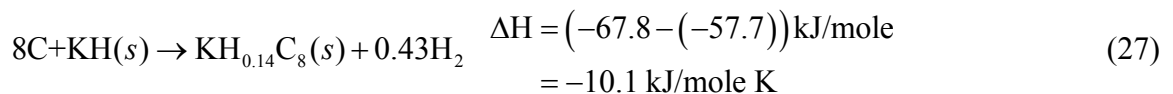
Then, the heat of formation of $KH_{0.14}C_8(s)$ is the sum of Eqs. (23) and (24):

$$\Delta H_f(KH_{0.14}C_8(s)) = (-33.5 + (-34.3)) \text{ kJ/mole K} = -67.8 \text{ kJ/mole K} \quad (25)$$

The heat of formation of KH is [60]:

$$\Delta H_f(KH) = -57.7 \text{ kJ/mole K} \quad (26)$$

Thus, the energy for the reaction to form potassium hydride graphite from KH is given by the differences in the heats of formation given by Eqs. (25) and (26):



Due to the marginally exothermic nature of the intercalation reaction, the regeneration may be achieved by heating wherein the metal may be dynamically removed to force the reaction further to completion. A suitable temperature for regeneration is in the range of about 500–700 °C. Specifically, the reaction product KHC_x was heated to over 550 °C, a temperature above which K intercalation does not occur [61], and the K metal vapor was condensed separately.

The third type of reaction to propagate hydrino formation was a hydride-exchange reaction between an alkali hydride NaH or KH and Mg or Li at elevated temperature wherein NaH, KH, and MgH_2 or LiH have complementary thermal decomposition temperatures with NaH and KH less stable than MgH_2 or LiH [53]:



The reaction of Eq. (28) is endothermic, but may proceed at the elevated temperature. The reaction of Eq. (29) is exothermic and is spontaneous above its activation temperature. During regeneration, the NaH or KH and MgH_2 or LiH of the reaction products were thermally decomposed, and Na or K metal vapor was condensed separately due to their much higher volatility. No intermetallic is formed between any combination of Na, K, Li, and Mg [62].

The fourth type of reaction was the dispersion of NaH on a support to form NaH molecules that are the catalyst and source of H to form hydrinos. Ordinarily, NaH has ionic bonding, but at elevated temperature on specific high-surface-area supports, the endothermic reaction given by Eq. (30) may occur to propagate the highly exothermic hydrino reaction given by Eqs. (11–14) at a high rate.



During regeneration, the NaH was thermally decomposed, and Na metal vapor was condensed. NaH may be added back to the regenerated support to reconstitute the reaction mixture to undergo the dispersion and hydrino reactions again.

Each reaction type formed predictable products based on the corresponding maximum heat release E_{mt} calculable from the known enthalpies of the reactants and products. The products were confirmed by XRD. The energy balance was measured by absolute water flow calorimetry. Additionally, significant energy excess E_{ex} was observed due to the formation of hydrinos with 50 MJ/mole of H₂ converted. The forward reaction is spontaneous at the reaction temperature, but it was shown that the equilibrium could be shifted from predominantly products to the reverse direction by dynamically removing a volatile reverse-reaction product such as an alkali metal. The isolated reverse-reaction products can be further reacted to form the initial reactants combined to form the initial reaction mixture. For example, in each class of hydrino propagating reaction, the metal hydride is trivially formed by the addition of H [63] to isolated metal. Then, the energy balance is zero except for thermal losses, the energy to replace the H converted to hydrino, and excess due the hydrino contribution. The former two are small <5% of E_{mt} and ~2% of E_{ex} considering electrolysis of water ($\Delta H_{H_2O(l)} = 285 \text{ kJ/mole}$) using electricity generated thermally with a 30% energy conversion factor; whereas, E_{ex} was observed to be more than 100% of E_{mt} . This is enabling of continuous generation of power with heat liberated by forming hydrinos as regeneration is concurrently maintained. The predicted molecular hydrino product H₂(1/4) was confirmed by solution ¹H NMR as shown in Sec. 3.3, and the corresponding hydrino hydride ion H⁻(1/4) was confirmed by XPS as shown in Sec. 3.4.

The four classes of hydride reactions may be maintained and regenerated in a batch mode using a thermally-coupled multi-cell array bundle wherein cells in the power-production phase of the cycle heat cells in the regeneration phase [64]. Alternatively, each cell can undergo both modes simultaneously [65]. In the intermittent design, the thermal power is statistically constant; whereas, in the latter it is directly constant. In both cases, the conversion of thermal power to electrical power requires the use of a heat engine exploiting a cycle such as a Rankine, Brayton, Stirling, or steam-engine cycle. Due to the temperatures, economy goal, and efficiency, the Rankine cycle is the most practical and can produce electricity at 30-40% efficiency with capital costs in the range of \$300/kW excluding the boiler component [64, 65].

2. Experimental

2.1. Catalyst Mixtures

Each reaction mixture comprised (i) a catalyst or source of catalyst and a source of hydrogen from the group of KH, and NaH, (ii) an oxidant from the group of MX_2 ($M = \text{Mg, Ca, Sr, Ba}$; $X = \text{F, Cl, Br, I}$), LiX ($X = \text{Cl, Br}$), and carbon, (iii) a reductant from the group of Mg, Ca, or Li and (iv) a support from the group of TiC, TiCN, Ti_3SiC_2 , WC nano, YC_2 , Pd/C, carbon black (CB), and LiCl reduced to Li. Compounds were from Sigma Aldrich, Alfa Aesar, Strem Chemicals, Inc, Accumet Material Co., Cerac Inc., and 3-One-2 LLC. The reactants were loaded in a glove box under an argon atmosphere and mixed by ball milling in hermetically sealed vessels or by using a blender in the glove box. The mixture was loaded in the cell in the glove box and the cell was sealed with a Swagelok cap or high-temperature valve.

The reactants, and their purity, vendors, and conditions of preparation are given in Table 2. For all reactants that could form a hydrate, the anhydrous compound was used when

commercially available. All supports, alkaline earth halides, and alkali halides were dried under vacuum at increasing temperatures and times until the water content was determined to be less than 10^{-5} moles/g by desorption studies using a physical gas parameter determination (P, V, T), mass spectroscopy, and quantitative gas chromatography as described previously [16, 17]. The halide-compound reactants were calorimetrically tested for the presence of trace water by the reaction of Mg (0.21 moles) with LiX or MX_2 (0.05 moles), and the energy was 0 kJ with experimental error. Quantitative X-ray diffraction (XRD) was performed on the starting materials and the reaction products using hermetically sealed sample holders (Bruker Model #A100B37) loaded in a glove box under argon, wax sealed, and analyzed with a Siemens D5000 diffractometer using Cu radiation at 40kV/30mA over the range $10^\circ - 70^\circ$ with a step size of 0.02° and a counting time of eight hours. All starting materials were 100% except that Ti_3SiC_2 was 88.9 wt% Ti_3SiC_2 and 11.1 wt% TiC. Mass spectroscopy and quantitative GC on the reaction product gases showed some methane with carbon supports that had a negligible impact on the heat balance.

2.2. Water-Flow, Batch Calorimetry

The cylindrical stainless steel reactors comprised approximately 95 cm³ volume (1.25" inside diameter (ID), 4.75" length, and 0.125" wall thickness), 130.3 cm³ volume (1.5" ID, 4.5" length, and 0.2" wall thickness), and 1988 cm³ volume (3.75" ID, 11" length, and 0.375" wall thickness). The water flow calorimeter comprised a vacuum chamber containing each cell and an external water coolant coil that collected 99+% of the energy released in the cell to achieve an error < ±1%. Both the cells and water-flow calorimeter were described previously [16, 17]. The energy recovery was determined by integrating the total output power P_T over time. The power was given by

$$P_T = \dot{m}C_p\Delta T \quad (31)$$

where \dot{m} was the mass flow rate, C_p was the specific heat of water, and ΔT was the absolute change in temperature between the inlet and outlet. The reaction was initiated by applying precision power to external resistive heaters. Specially, 100–200 W of power (130.3 cm³ cell) or 800–1000 W (1988 cm³ cell) was supplied to the heater. During this heating period, the reagents reached a temperature threshold wherein the onset of the hydrino reaction was typically confirmed by a rapid rise in cell temperature. Once the cell temperature reached a desired maximum temperature (Table 3) the input power was set to zero. To increase the rate of heat transfer to the coolant, the chamber was re-pressurized with 1000 Torr of helium as described previously [16, 17], and the maximum change in water temperature (outlet minus inlet) was approximately 1.2 °C. The assembly was allowed to fully reach equilibrium over a 24-hour period as confirmed by the observation of full equilibrium in the flow thermistors.

2.3. Regeneration Reactions

Alkaline earth or lithium halides were formed by reacting an alkaline earth metal or lithium hydride (or lithium) with the corresponding alkali halide. The reactant loadings, reaction conditions, and XRD results are given in Table 4. Typically, a two-to-one molar mixture of alkali halide and alkaline earth metal or a one-to-one molar mixture of alkali halide and Li or LiH were placed in the bottom of a crucible made with a ~25.4 cm long, 1.27–1.9 cm OD stainless steel (SS) tube (open at one end) in a 2.54 cm OD vacuum-tight quartz tube (open at one end). The open end of the SS tube was placed about ~2.54 cm outside of the furnace such that any alkali metal formed during the reaction cooled and condensed outside the heating zone to avoid any corrosion reaction between the alkali metal and quartz tube. The setup was oriented horizontally to increase the surface area of the heated chemicals. The reaction was run at 700–850 °C for 30 minutes either under vacuum, or under 1 atm of Ar gas followed by evacuating the alkali metal for 30 minutes at a similar temperature. In another setup, the reactants were placed in the SS crucible, and the melt was sparged (10 sccm) with dry Ar for mixing. The Ar was supplied through a needle having its opening at the bottom of the melt. Alkali metal was evaporated from the hot zone. After reaction, the reactor was cooled down to room temperature and transferred to a glove box for product collection. XRD was used to identify the product. The sample was prepared in a glove box by pulverizing the product and loading it into a panalytical holder that was sealed with a plastic cover film.

Pd/C was regenerated from the reaction product KHC_x by heating the product of the reaction mixture 8.3g KH + 12g Pd/C in a stainless steel gas cell according to the methods described previously [16, 17]. The reactor was run at 550 °C in a kiln for 96 hours. The K metal vapor was condensed in the 1.27 cm ID vacuum line at room temperature. Then, the reactor was

cooled under helium atmosphere. The sealed reactor was then opened in a glove box under an argon atmosphere. The product material was analyzed by XRD.

The reaction mixtures of 5g NaH + 5g Mg + 20g TiC, 8.3g KH + 5g Mg + 20g TiC, 5g NaH + 5g Mg + 20g TiC + 0.35g Li, 8.3g KH + 5g Mg + 20g TiC + 0.35g Li, NaH + 20g TiC + 0.35g Li, 8.3g KH + 20g TiC + 0.35g Li, and 5g NaH + 20g TiC were regenerated by heating the product at 600 °C, 500 °C, 750 °C, 750 °C, 750 °C, 750 °C, and 500 °C, respectively, under vacuum for 30 minutes using the procedure for KHC_x . The resulting TiC and metal bands were analyzed by XRD.

2.4. Solution NMR

50 mg of reaction product was added to 1.5 ml of deuterated N,N-dimethylformamide-d7 ($\text{DCON}(\text{CD}_3)_2$), DMF-d7 (99.5% Cambridge Isotope Laboratories, Inc.) in a vial that was sealed with a glass Teflon valve, agitated, and allowed to dissolve over a 12 hour-period in a glove box under an argon atmosphere. The solution in the absence of any solid was transferred to an NMR tube (5 mm OD, 23 cm length, Wilmad) by a gas-tight connection, followed by flame-sealing of the tube. Additionally, control NMR samples comprised the starting materials added to NMR solvent with the dissolved portion analyzed. The NMR spectra were recorded with a 500 MHz Bruker NMR spectrometer that was deuterium locked. The chemical shifts were referenced to the solvent frequency such as DMF-d7 at 8.03 ppm relative to Tetramethylsilane (TMS).

2.5. XPS Spectra

A series of XPS analyses were made on the product and control reactant samples using a Scienta 300 XPS Spectrometer. The samples were loaded into the XPS using an Ar filled glove

box without exposure to air. The fixed analyzer transmission mode and the sweep acquisition mode were used. The step energy in the survey scan was 0.5 eV, and the step energy in the high-resolution scan was 0.15 eV. In the survey scan, the time per step was 0.4 seconds, and the number of sweeps was 4. In the high-resolution scan, the time per step was 0.3 seconds, and the number of sweeps was 30. $C\ 1s$ at 284.5 eV was used as the internal standard.

3. Results and Discussion

3.1. Water-Flow Calorimetry Power Measurements

The maximum energetic reaction, XRD results, experimental net energy E_{net} , energy released per mole ΔH of alkaline earth or alkali halide or per mole of H for hydrino reactions given by Eqs. (19–20), (22) and (28–30), respectively, calculated theoretical maximum energy E_{mt} for conventional chemistry [66–68], excess heat from the hydrino reaction E_{ex} , maximum temperature of run T , and energy gain G of hydrino catalyst systems comprising reactants chosen from (i) NaH or KH, (ii) Mg, Ca, or Li, and (iii) MX_2 ($M = Mg, Ca, Sr, Ba; X = F, Cl, Br, I$), LiX ($X = Cl, Br$) or LiX ($X = Cl, Br$) and (iv) TiC, TiCN, Ti_3SiC_2 , WC, YC_2 , Pd/C, carbon black (CB), and LiCl are given in Table 3. In each test, the energy input and energy output were calculated by integration of the corresponding power as described previously [16, 17]. The thermal energy in the coolant flow in each time increment was calculated using Eq. (31) by multiplying volume flow rate of water by the water density at 19 °C (0.998 kg/liter), the specific heat of water (4.181 kJ/kg °C), the corrected temperature difference, and the time interval. Values were summed over the entire experiment to obtain the total energy output. The total energy from the cell E_T must equal the energy input E_{in} and any net energy E_{net} . Thus, the net energy was given by

$$E_{net} = E_T - E_{in} \quad (32)$$

From the energy balance, any excess heat E_{ex} was determined relative to the maximum theoretical E_{mt} by

$$E_{ex} = E_{net} - E_{mt} \quad (33)$$

The calibration test results demonstrated a heat coupling of better than 98% of the resistive input to the output coolant, and zero excess heat controls demonstrated that with the calibration correction applied, the calorimeter was accurate to within less than 1% error [16, 17]. In addition, the control decomposition reaction of NH_4NO_3 to N_2O and H_2O and the control reaction of $\text{Mg} + \text{Fe}_2\text{O}_3$ to MgO were about 92% and 94%, respectively, of the maximum theoretical energy indicating that applying the maximum theoretical energy is a conservative approach [17].

Using a method of determining the reaction time for which the excess energy reached a limit as the reaction time was increased, the reaction durations for completion were between one and 10 minutes. Typical parameters (Table 3) measured by absolute water-flow calorimetry for the halide hydride exchange reaction of NaH or KH with alkaline earth halides MX_2 or LiX were 2–5 times energy gain relative to regeneration chemistry, 7 Wcm^{-3} , and 300–400 kJ/mole oxidant with a cell operation temperature of about 400–750 °C. A representative XRD of the reaction product of 8.3g $\text{KH} + 5\text{g Mg} + 20\text{g TiC} + 2.13\text{g LiCl}$ under these conditions is shown in Figure 1. Further energy gain can be obtained by optimizing the reactants ratios from the standard amounts used for comparison purposes. For example, by changing the amount of SrCl_2 from 0.05 moles to 0.03 moles, the energy gain increased from 2.4 to 3.5 times E_{mt} . Similar results were obtained with other supports such as TiCN , Ti_3SiC_2 , WC , YC_2 , and Pd/C . In the latter case, Pd/C served as a support for NaH since Na does not form an intercalation compound with carbon

[69]. Supports with low surface area and nonconducting (results not given in Table 3) gave no excess heat. In the halide-hydride exchange reaction, LiCl is reduced to Li that can serve as the conducting support. It was observed that the excess heat was reduced about 30% with the absence of a carbide support with LiCl present, but it was still appreciable. As long as oxygen and the reactor corrosion products are avoided, the reactions were found to be reversible through a repeat cycle. The surface area of the support such as TiC determined by the BET method was retained to within at least 90% with temperature cycling to 750 °C, but degradation of surface area is expected over many regenerative cycles. Systems not requiring a support are under development.

The parameters acquired on the system 8.3 g KH + 12 g Pd/C and 42.0 g KH + 25.0 g Mg + 100.0 g CB wherein carbon served as the oxidant in place of MX₂ are shown in Table 3. The maximum theoretical energy is calculated in Sec. 1.2. There was excess heat of 9.9 kJ was observed with Pd/C, and hydride products were formed in a representative run as shown in Secs. 3.3 and 3.4. A summary of the thermal parameters are 8.6 times energy gain relative to regeneration chemistry, 2.1 W cm⁻³, and 54.0 kJ/mole KH with a cell operation temperature of about 571 °C. The regeneration time of carbon-intercalated compounds is excessive [70], and residue alkali metal remains [71]. Intercalated K was removed by evacuation of the intercalation product at 550 °C in a kiln for 96 hours until K metal no longer condensed. The regeneration of Pd/C was confirmed by XRD.

The parameters acquired on the system 5g NaH or 8.3 g KH + 5 g Mg + 20 g TiC involving a hydride exchange between NaH or KH and Mg are shown in Table 3. The maximum theoretical energy is endothermic. Higher temperatures were required to obtain substantial excess heat in the absence of the alkaline earth or alkali halide. Thus, the exothermic halide-

hydride exchange reaction may further provide activation energy to the hydride reaction. A summary of the thermal parameters are infinite energy gain relative to regeneration chemistry, 1.7 W cm^{-3} , and about 30 kJ/mole hydride with a cell operation temperature of about 550 °C. A summary of the thermal parameters acquired on the system 5g NaH or 8.3 g KH + 5 g Mg + 20 g TiC + 0.35g Li or 5g NaH or 8.3 g KH + 20 g TiC + 0.35g Li involving a hydride exchange between NaH or KH and Li is about 6 times energy gain relative to regeneration chemistry, 2.8 W cm^{-3} , and about 48 kJ/mole hydride starting material with a cell operation temperature of about 550 °C. Both Mg and Li systems were trivially regenerated in about 20 minutes by heating the products of the reactants of 5g NaH + 5g Mg + 20g TiC, 8.3g KH + 5g Mg + 20g TiC, 5g NaH + 5g Mg + 20g TiC + 0.35g Li, 8.3g KH + 5g Mg + 20g TiC + 0.35g Li, NaH + 20g TiC + 0.35g Li, 8.3g KH + 20g TiC + 0.35g Li, and 5g NaH + 20g TiC at 600 °C, 500 °C, 750 °C, 750 °C, 750 °C, 750 °C, and 500 °C, respectively under vacuum with condensation of the metals in separate regions of a temperature gradient. The separable metals and the immiscibility of alkali and alkaline earth metals make these favorable regenerable chemical systems for a commercial power plant.

The parameters acquired on the system 5 g NaH + 20 g TiC involving a dispersion reaction of NaH on TiC is shown in Table 3. The maximum theoretical energy is zero. A summary of the thermal parameters are infinite energy gain relative to regeneration chemistry, 1.4 W cm^{-3} , and about 24 kJ/mole hydride with a cell operation temperature of about 580 °C. The system was trivially regenerated in about 20 minutes by heating at 600 °C under vacuum with condensation of Na.

3.2. Hydride-Halide Regeneration Reaction Results

The halide-hydride exchange reaction between KH and MX_2 or LiX is spontaneous in a closed system with the reaction going essentially to completion with excess energy E_{ex} produced as given in Table 3. To demonstrate the thermal reversibility of the products to reactants, the system was changed to an open one. Reacting an alkaline earth metal or LiH with the corresponding potassium halide while potassium metal was evaporated from the hot zone and condensed separately, formed alkaline earth halides or lithium halides. The reactant amounts, temperature, duration, and XRD results are given in Table 4. Since the duration of the forward reaction is as short as a minute whereas that of the regeneration is significantly longer, the power and cost of a commercial power system can be optimized with a chemistry that has a fast regeneration time and high yield of a pure compound. For magnesium, only the fluoride could be regenerated, and in some cases complexes with KX were formed under the reaction conditions. Considering that the oxidized product is due to the leakiness of the XRD holder to air, SrBr₂ and LiCl or LiBr are very favorable candidates having essentially 100% yield in 30 minutes. Regeneration results of the other three chemistry types are given in Sec. 3.1.

The four classes of chemistries involving exchange reactions or a dispersion reaction that propagate the production of hydrinos demonstrated the release of energy E_{ex} that was at least as large as the energies E_{mt} of the former reactions. These reactions were shown to be thermally reversible to permit the regeneration of the initial reactants to run the next power cycle with add back of a small amount of hydrogen to replace that consumed to form hydrinos. The net energy of the overall cycle is essentially E_{ex} as demonstrated for the exemplary mass and energy balance for the reactants KH Mg TiC SrBr₂.

3.2.1. Step 1

TiC is non-reactive as confirmed by XRD of the products, and the maximum theoretical energy for the reaction of the initial reactants involves only KH and SrBr₂. The energy is



Hydrinos are formed in this step with release of additional energy E_{ex} shown in Table 3. The hydrino product H₂(1/4) was also confirmed by isolation and analysis by techniques such as proton NMR. Based on E_{ex} and the 50 MJ/mole heat of reaction to form H₂(1/4) from H₂, the hydrogen consumed to form hydrino is less than 1% of the hydrogen inventory. Then, only the halide and hydride reaction and regeneration chemistries need be considered to determine the overall mass and energy balance. Typically, these reactants can be regenerated from the products by isolation, molten salt electrolysis, and reactions to form the original reactants. However, it is demonstrated in this paper that the selected reactants can be regenerated by a direct thermal method that consumes far less energy, only the energy of the forward reaction by forcing the reverse reaction.

3.2.2. Step 2

Pumping off hydrogen to decompose SrH₂ absorbs heat of the amount:



3.2.3. Step 3

Switching from a closed to an open system allows for the thermal reverse reaction (Table 4):



wherein the reaction is driven to completion by dynamically evaporating potassium as K(g).

3.2.4. Step 4

Separately, K is condensed and the heat of vaporization is recovered.

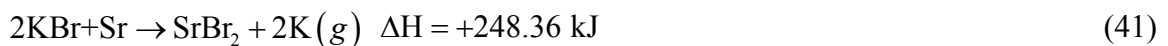
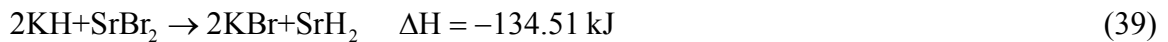


The heat of hydriding K to KH is also recovered:



The SrBr₂ (Step 3) and KH (Step 4) are recombined to complete the energy neutral cycle giving the original reactants at the original temperature.

3.2.5. Overall mass and energy balance for hydrino production reaction and regeneration steps



In operation, minor losses are incurred due to irrecoverable heat losses not to the load and small H₂ pumping losses. Also, the H converted to hydrino H must be replaced. These former losses should be conservatively a few percent based on existing power plants. The latter is about 1–2% of the heat released to form hydrino since the heat of formation of hydrino is –50 MJ/mole H₂ (1/4) compared to the heat of formation of hydrogen from liquid water of

+285 kJ/mole H₂. The energy from hydrino formation from less than 1% of the hydrogen inventory is hundreds of percent that of the conventional chemistry (hydride-halide exchange) and can be used to power applications. A practical design would utilize the elevated temperature from power producing cells to transfer heat to the regenerating cells as the cycle is controlled to maintain constant power output [64]. In the case of large energy gains, supplemental electrical-powered heat to elevate cell temperatures is practical, especially with the use of a heat recuperator. In other designs under development, each cell produces continuous power by controlling the mass and energy flow within each cell, and the power is scaled according to the number of cells [65].

3.3. NMR Identification of H₂(1/4)

The isolation and identification of the predicted molecular hydrino product H₂(1/4) was pursued by extraction of these molecules from reaction products into the NMR solvent d-DMF. Confirmation of this product was achieved with the observation of the H₂(1/4) peak at about 1.2 ppm from many representative reaction mixtures as shown in shown in Figures 2–12. Using Eq. (18) and the experimental absolute resonance shift of TMS, -31.5 ppm, the predicted gas-phase shift of H₂(1/4) is

$$\frac{\Delta B_T}{B} = -30.6\text{ppm} - (-31.5\text{ppm}) = 0.9\text{ppm} \quad (45)$$

which is very close to the observed shift of 1.2 ppm. Furthermore, the experimental absolute H₂ gas-phase resonance shift of -28.0 ppm is in excellent agreement with the predicted absolute gas-phase shift of -28.01 ppm (Eq. (18)) as given in Sec. 1.1. These solution-phase results match prior results and not only provide the possibility of an unequivocal identification of H₂(1/4), but their characteristics of having the absence of any solid matrix effect or the possibility of

alternative assignments such as U-centered H or F centers in solid matrix confirm the prior solid NMR assignments as well [16, 17].

3.3. XPS Identification of $H^{-}(1/4)$

A survey spectrum was obtained over the region $E_b = 0$ eV to 1200 eV (Figure 13) on the reaction product of 8.3g KH + 5g Mg + 20g TiC that produced an excess energy of 8.42 kJ. The primary element peaks allowed for the determination of all of the elements present. No elements were present in the survey scan which could be assigned to peaks in the low binding energy region (Figure 14) with the exception of the K $3p$ peak at 17 eV, K $3s$ at 33 eV, Mg $2p$ at 50 eV, Ti $3s$ at 59 eV, and the Mg $2s$ at 89 eV. Accordingly, any other peaks in this region must be due to novel species. As shown in Figure 14, the XPS spectrum differs from the known peaks due to the identified primary elements having additional peaks at 9.3 eV and 11.2 eV, but these do match the $H^{-}(1/4)$ $E_b = 11.2$ eV hydride ion (Eq. (10)). The literature was searched for elements having a peak in the valence-band region that could be assigned to these peaks. Given the primary element peaks present, there was no known alternative assignment. Thus, the 9.3 eV and 11.2 eV peaks that could not be assigned to known elements and do not correspond to any other primary element peak were assigned to the $H^{-}(1/4)$ in two different chemical environments. These features closely matched those for $H^{-}(1/4)$ of KH*I reported previously [16–18, 33–35]. The presence of $H^{-}(1/4)$ in two different chemical environments is further evidenced by the 1H MAS NMR spectrum such as that of KH*Cl shown in Figure 49 compared to Figure 35A of Ref. [17].

A survey spectrum was obtained over the region $E_b = 0$ eV to 1200 eV (Figure 15) on the reaction product of 8.3g KH + 12g Pd/C that produced an excess energy of 9.94 kJ. The primary element peaks allowed for the determination of all of the elements present. No elements were present in the survey scan which could be assigned to peaks in the low binding energy region (Figure 16) with the exception of the K $3p$ peak at 17 eV and K $3s$ at 33 eV. Accordingly, any other peaks in this region must be due to novel species. As shown in Figure 16, the XPS spectrum differs from the known peaks due to the identified primary elements having additional peaks at 8.9 eV and 10.7 eV, but these do match the $H^- (1/4)$ $E_b = 11.2$ eV hydride ion (Eq. (10)). Given the primary element peaks present, there was no known alternative assignment. Thus, the 8.9 eV and 10.7 eV peaks that could not be assigned to known elements and do not correspond to any other primary element peak were assigned to the $H^- (1/4)$ in two different chemical environments.

4. Conclusion

The energy balance for representative power and regeneration reactions of four classes of hydrino catalyst systems were tested. Significant excess power and high thermal regeneration kinetics and high yield were obtained on multiple chemical systems. Each system comprised a thermally-reversible reaction mixture of a catalyst or source of catalyst and a source of hydrogen (KH or NaH), a high-surface-area conductive support (TiC, TiCN, Ti_3SiC_2 , WC, YC_2 , Pd/C, carbon black (CB), and LiCl reduced to Li), and a reductant (Mg, Ca, or Li). Additionally, two systems comprised an alkaline earth or alkali halide oxidant, or the carbon support comprised the oxidant. The reactions to propagate hydrino formation were (i) (a) an oxidation-reduction reaction involving hydride-halide exchange between NaH or KH and an alkaline earth halide or

alkali halide (Eq. (19–20)), or (b) carbon served as the oxidant during the reaction with KH to form the intercalation compound KHC_x (Eq. (22)), (ii) a hydride exchange reaction (Eqs. (28–29)) between NaH or KH and Mg or Li, and (iii) a dispersion reaction of NaH on a support (Eq. (30)). The forward reaction was spontaneous at the test conditions. But, it was shown that the equilibrium could be shifted from predominantly the products to the reverse direction by dynamically removing the volatile reverse-reaction product, the alkali metal, during a separate regeneration reaction. Specifically, for case (i)(a), the alkaline earth halides or lithium halides were formed by the reaction of the corresponding alkaline earth metal or LiH and Na or K halide at elevated temperature (650–800 °C) as the alkali metal was evaporated and separately condensed. For case (i)(b), the reaction product KHC_x was heated to over 550 °C, a temperature above which K intercalation does not occur [61], and the K metal vapor was condensed separately. For case (ii), NaH or KH and MgH_2 or LiH of the reaction products were thermally decomposed, and Na or K metal vapor was condensed separately. For case (iii), NaH on TiC was thermally decomposed, and Na metal vapor was condensed separately. The metal hydride is trivially formed by the addition of H [63].

In general, these reactions demonstrate that hydrinos may be formed using a thermally reversible reaction of a catalyst or source of catalyst, a source of hydrogen, and at least one other reactant to form predictable products based on the corresponding maximum heat release E_{mt} calculable from the known enthalpies of the reactants and products. Additionally, significant energy excess E_{ex} is due to the formation of hydrinos with 50 MJ/mole of H_2 converted. For the power and regeneration cycle, the energy balance is zero except for thermal losses, the energy to replace the H converted to hydrino, and the excess due to the hydrino contribution. The former two are small <5% of E_{mt} and ~2% of E_{ex} considering electrolysis of water

($\Delta H_{\text{H}_2\text{O}(\ell)} = 285 \text{ kJ/mole}$) using electricity generated thermally with a 30% energy conversion factor; whereas, E_{ex} was observed to be more than 100% of E_{in} .

Thus, the energy gain due to hydrino formation measured by absolute water-flow calorimetry was greater than that of the hydrino propagation reaction at power-plant operating conditions. Then, the thermal cycle of reactants to products thermally reversed to reactants is energy neutral, the thermal losses and energy to replace hydrogen converted to hydrinos are relatively small, and the total energy released is multiples of the conventional chemical energy due to the contribution of hydrino formation. At least two of the four reaction systems are enabling of continuous generation of power liberated by forming hydrinos using simplistic and efficient systems that concurrently maintain regeneration as part of the thermal energy balance [64, 65]. The system is closed except that only hydrogen consumed in forming hydrinos needs to be replaced. The predicted molecular hydrino product $\text{H}_2(1/4)$ was confirmed by solution ^1H NMR. It is a nonpolluting product due to its extraordinarily stability that cannot be contained in the atmosphere as is the case for ordinary hydrogen. These results demonstrate a new non-polluting power source.

References

1. R.L. Mills, The Grand Unified Theory of Classical Physics; June 2010 Edition, posted at <http://www.blacklightpower.com/theory/bookdownload.shtml>.
2. R.L. Mills, B. Holverstott, B. Good, N. Hogle, A. Makwana, Total Bond Energies of Exact Classical Solutions of Molecules Generated by Millsian 1.0 Compared to Those Computed Using Modern 3-21G and 6-31G* Basis Sets, *Phys. Essays* 23, (2010) 153–199.
3. W. Xie, R.L. Mills, W. Good, A. Makwana, B. Holverstott and N. Hogle, Millsian 2.0: A Molecular Modeling Software for Structures, Charge Distributions and Energetics of Biomolecules, *Physics Essays*, 24 (2011) 200–212.
4. R. L. Mills, Classical Quantum Mechanics, *Phys. Essays* 16 (2003) 433–498.
5. R. Mills, Physical Solutions of the Nature of the Atom, Photon, and Their Interactions to Form Excited and Predicted Hydrino States, *Phys. Essays* 20 (2007) 403–460.
6. R. L. Mills, Exact Classical Quantum Mechanical Solutions for One- Through Twenty-Electron Atoms, *Phys. Essays* 18 (2005) 321–361.
7. R. L. Mills, The Nature of the Chemical Bond Revisited and an Alternative Maxwellian Approach, *Phys. Essays* 17 (2004) 342–389.
8. R. L. Mills, Maxwell's Equations and QED: Which is Fact and Which is Fiction, *Phys. Essays* 19 (2006) 225–262.
9. R. L. Mills, Exact Classical Quantum Mechanical Solution for Atomic Helium Which Predicts Conjugate Parameters from a Unique Solution for the First Time, *Phys. Essays* 21 (2008) 103–141.
10. R. L. Mills, The Fallacy of Feynman's Argument on the Stability of the Hydrogen Atom According to Quantum Mechanics, *AFLB* 30 (2005) 129–151.

11. R. Mills, The Grand Unified Theory of Classical Quantum Mechanics, *Int. J. Hydrogen Energy*, 27 (2002) 565–590.
12. R. Mills, The Nature of Free Electrons in Superfluid Helium—a Test of Quantum Mechanics and a Basis to Review its Foundations and Make a Comparison to Classical Theory, *Int. J. Hydrogen Energy* 26 (2001) 1059–1096.
13. R. Mills, The Hydrogen Atom Revisited, *Int. J. Hydrogen Energy* 25 (2000) 1171–1183.
14. R. L. Mills, Y. Lu, K. Akhtar, Spectroscopic Observation of Helium-Ion- and Hydrogen-Catalyzed Hydrino Transitions, *Cent. Eur. J. Phys.* 8 (2010) 318–339 .
15. R. L. Mills and Y. Lu, Hydrino Continuum Transitions with Cutoffs at 22.8 nm and 10.1 nm, *Int. J. Hydrogen Energy*, 35 (2010) 8446–8456.
16. R.L. Mills, K. Akhtar, G. Zhao, Z. Chang, J. He, X. Hu, G. Chu, Commercializable Power Source Using Heterogeneous Hydrino Catalysts, *Int. J. Hydrogen Energy* 35 (2010) 395–419.
17. R. L. Mills, G. Zhao, K. Akhtar, Z. Chang, J. He, Y. Lu, W. Good, G. Chu, B. Dhandapani, Commercializable Power Source from Forming New States of Hydrogen, *Int. J. Hydrogen Energy* 34, (2009), 573–614.
18. R. Mills, P. Ray, B. Dhandapani, W. Good, P. Jansson, M. Nansteel, J. He, A. Voigt, Spectroscopic and NMR Identification of Novel Hydride Ions in Fractional Quantum Energy States Formed by an Exothermic Reaction of Atomic Hydrogen with Certain Catalysts, *Eur. Phys. J.–Appl. Phys.* 28 (2004) 83–104.
19. K. Akhtar, J. Scharer, R. L. Mills, Substantial Doppler broadening of atomic-hydrogen lines in DC and capacitively coupled RF plasmas, *J. Phys. D, Appl. Phys.* 42 (2009) 135207.
20. R. Mills, K. Akhtar, Tests of Features of Field-Acceleration Models for the Extraordinary Selective H Balmer α Broadening in Certain Hydrogen Mixed Plasmas, *Int. J. Hydrogen*

- Energy 34 (2009) 6465–6477.
21. R. L. Mills, P. Ray, B. Dhandapani, R. M. Mayo, J. He, Comparison of Excessive Balmer α Line Broadening of Glow Discharge and Microwave Hydrogen Plasmas with Certain Catalysts, *J. Appl. Phys.* 92 (2002) 7008–7022.
 22. R. L. Mills, P. Ray, B. Dhandapani, J. He, Comparison of Excessive Balmer α Line Broadening of Inductively and Capacitively Coupled RF, Microwave, and Glow Discharge Hydrogen Plasmas with Certain Catalysts, *IEEE Trans. Plasma Sci.* 31 (2003) 338–355.
 23. R. L. Mills, P. Ray, Substantial Changes in the Characteristics of a Microwave Plasma Due to Combining Argon and Hydrogen, *New J. Phys.*, www.njp.org, 4, (2002) 22.1–22.17.
 24. R. L. Mills, B. Dhandapani, K. Akhtar, Excessive Balmer α Line Broadening of Water-Vapor Capacitively-Coupled RF Discharge Plasmas, *Int. J. Hydrogen Energy* 33 (2008) 802–815.
 25. R. Mills, P. Ray, B. Dhandapani, Evidence of an Energy Transfer Reaction Between Atomic Hydrogen and Argon II or Helium II as the Source of Excessively Hot H Atoms in RF Plasmas, *J. Plasma Phys.* 72 (2006) 469–484.
 26. J. Phillips, C-K Chen, K. Akhtar, B. Dhandapani, R. Mills, Evidence of Catalytic Production of Hot Hydrogen in RF Generated Hydrogen/Argon Plasmas, *Int. J. Hydrogen Energy* 32 (2007) 3010–3025.
 27. R. L. Mills, P. C. Ray, R. M. Mayo, M. Nansteel, B. Dhandapani, J. Phillips, Spectroscopic Study of Unique Line Broadening and Inversion in Low Pressure Microwave Generated Water Plasmas, *J. Plasma Phys.* 71 (2005) 877–888.
 28. R. L. Mills, K. Akhtar, Fast H in Hydrogen Mixed Gas Microwave Plasmas when an Atomic Hydrogen Supporting Surface Was Present, *Int. J. Hydrogen Energy*, 35 (2010) 2546–2555.

29. D. R. Lide, CRC Handbook of Chemistry and Physics, 86th Edition, CRC Press, Taylor & Francis, Boca Raton, (2005–6), pp. 9-54 to 9-59.
30. D. R. Lide, CRC Handbook of Chemistry and Physics, 86th Edition, CRC Press, Taylor & Francis, Boca Raton, (2005–6), pp. 10-202 to 10-204.
31. R. L. Mills, P. Ray, A Comprehensive Study of Spectra of the Bound-Free Hyperfine Levels of Novel Hydride Ion $H^- (1/2)$, Hydrogen, Nitrogen, and Air, Int. J. Hydrogen Energy 28 (2003) 825–871.
32. R. Mills, Spectroscopic Identification of a Novel Catalytic Reaction of Atomic Hydrogen and the Hydride Ion Product, Int. J. Hydrogen Energy 26 (2001) 1041–1058.
33. R. Mills, B. Dhandapani, M. Nansteel, J. He, T. Shannon, A. Echezuria, Synthesis and Characterization of Novel Hydride Compounds, Int. J. Hydrogen Energy 26, (2001) 339–367.
34. R. Mills, B. Dhandapani, M. Nansteel, J. He, A. Voigt, Identification of Compounds Containing Novel Hydride Ions by Nuclear Magnetic Resonance Spectroscopy, Int. J. Hydrogen Energy 26 (2001) 965–979.
35. R. Mills, B. Dhandapani, N. Greenig, J. He, Synthesis and Characterization of Potassium Iodo Hydride, Int. J. Hydrogen Energy 25 (2000) 1185–1203.
36. K. R. Lykke, K. K. Murray, W. C. Lineberger, Threshold photodetachment of H^- , Phys. Rev. A 43 (1991) 6104–6107.
37. K. K. Baldrige, J. S. Siegel, Correlation of empirical δ (TMS) and absolute NMR chemical shifts predicted by ab initio computations, J. Phys. Chem. A 103 (1999) 4038–4042.
38. J. Mason, Editor, Multinuclear NMR, Plenum Press, New York, (1987), Chp. 3.

39. C. Suarez, E. J. Nicholas, M. R. Bowman, Gas-phase dynamic NMR study of the internal rotation in N-trifluoroacetlypyrrolidine, *J. Phys. Chem. A* 107 (2003) 3024–3029.
40. C. Suarez, Gas-phase NMR spectroscopy, *The Chem. Educator* 3, No. 2 (1998) 1–18.
41. R. Mills and M. Nansteel, P. Ray, Argon-Hydrogen-Strontium Discharge Light Source, *IEEE Trans. Plasma Sci.* 30 (2002) 639–653.
42. R. Mills and M. Nansteel, P. Ray, Bright Hydrogen-Light Source due to a Resonant Energy Transfer with Strontium and Argon Ions, *New J. Phys.* 4 (2002) 70.1–70.28.
43. R. Mills, J. Dong, Y. Lu, Observation of Extreme Ultraviolet Hydrogen Emission from Incandescently Heated Hydrogen Gas with Certain Catalysts, *Int. J. Hydrogen Energy* 25 (2000) 919–943.
44. R. Mills, M. Nansteel, P. Ray, Excessively Bright Hydrogen-Strontium Plasma Light Source Due to Energy Resonance of Strontium with Hydrogen, *J. Plasma Phys.* 69 (2003) 131–158.
45. R. L. Mills, J. He, M. Nansteel, B. Dhandapani, Catalysis of Atomic Hydrogen to New Hydrides as a New Power Source, *IJGEI, Special Edition in Energy Systems*, 28, Nos. 2/3 (2007) 304–324.
46. H. Conrads, R. Mills, Th. Wrubel, Emission in the Deep Vacuum Ultraviolet from a Plasma Formed by Incandescently Heating Hydrogen Gas with Trace Amounts of Potassium Carbonate, *Plasma Sources Sci. Technol.* 12, (2003) 389–395.
47. J. Phillips, R. L. Mills, X. Chen, Water Bath Calorimetric Study of Excess Heat in ‘Resonance Transfer’ Plasmas, *J. Appl. Phys.* 96 (2004) 3095–3102.
48. R. L. Mills, Y. Lu, Time-resolved Hydrino Continuum Transitions with Cutoffs at 22.8 nm and 10.1 nm. Submitted for publication.

49. R. Mills, P. J. Lotoski, G. Zhao, K. Akhtar, Z. Chang, J. He, X. Hu, G. Wu, G. Chu, Y. Lu, Identification of New Hydrogen States, *Physics Essays*, 24 (2011) 95–117.
50. R. Mills, P. Ray, R. M. Mayo, CW HI Laser Based on a Stationary Inverted Lyman Population Formed from Incandescently Heated Hydrogen Gas with Certain Group I Catalysts, *IEEE Trans. Plasma Sci.* 31 (2003) 236–247.
51. R. L. Mills, P. Ray, Stationary Inverted Lyman Population Formed from Incandescently Heated Hydrogen Gas with Certain Catalysts, *J. Phys. D, Appl. Phys.* 36 (2003) 1504–1509.
52. R. Mills, P. Ray, R. M. Mayo, The Potential for a Hydrogen Water-Plasma Laser, *Appl. Phys. Letts.* 82 (2003) 1679–1681.
53. W. M. Mueller, J. P. Blackledge, G. G. Libowitz, *Metal Hydrides*, Academic Press, New York, (1968).
54. F. A. Cotton, G. Wilkinson, C. A. Murillo, M. Bochmann, *Advanced Inorganic Chemistry*, Sixth Edition, John Wiley & Sons, Inc., New York, (1999), pp. 92–93.
55. D. R. Lide, *CRC Handbook of Chemistry and Physics*, 86th Edition, CRC Press, Taylor & Francis, Boca Raton, (2005–6), p. 4–70.
56. D. R. Lide, *CRC Handbook of Chemistry and Physics*, 86th Edition, CRC Press, Taylor & Francis, Boca Raton, (2005–6), p. 6–58.
57. T. Enoki, S. Miyajima, M. Sano, H. Inouchi, Hydrogen-alkali-metal-graphite ternary intercalation compounds, *J. Mater. Res.* 5 (1990) 435–466.
58. M. S. Dresselhaus, G. Dresselhaus, Intercalation Compounds of Graphite, *Adv. Phys.* 51 (2002) 1–186.
59. J. Sangster, C-K (Carbon-Potassium) System, *J. Phase Equil. Diff.* 29 (2008) 73–83.

60. D. R. Lide, CRC Handbook of Chemistry and Physics, 86th Edition, CRC Press, Taylor & Francis, Boca Raton, (2005–6), pp. 5–13.
61. D. E. Nixon, G. S. Parry, Formation and structure of the potassium graphites, Brit. J. Appl. Phys. (J. Phys. D), Ser. 2, Vol. 1, (1968), 291–298.
62. W. F. Gale, T. C. Totemeier, Smithells Metals Reference Book, 8th Edition, Burlington, MA: Elsevier Butterworth-Heinemann, (2004).
63. G. Brauer, Editor, Handbook of Preparative Inorganic Chemistry, Second Edition, Academic Press, New York, New York, (1963) pp. 971–974.
64. R. L. Mills, G. Zhao, W. Good, M. Nansteel, Design for a BlackLight Power Multi-Cell Thermally Coupled Reactor Based on Hydrogen Catalyst Systems, submitted for publication. Available at <http://www.blacklightpower.com/pdf/ThermallyCoupled.pdf>.
65. R. Mills, G. Zhao, W. Good, Continuous Thermal Power System, Appl. Energy, 88 (2011) 789–798..
66. D. R. Lide, CRC Handbook of Chemistry and Physics, 88th Edition, CRC Press, Taylor & Francis, Boca Raton, (2007–8).
67. J. A. Dean, Lange's Handbook of Chemistry, 15th Edition, McGraw-Hill Professional, New York, (1999).
68. O. Knacke, O. Kubascheeski, K. Hesselmann, Thermochemical Properties of Inorganic Substances, 2nd Ed., Springer-Verlag Berlin, Heidelberg 1991.
69. Y. N. Novikov, M. E. Vol'pin, Lamellar compounds of graphite with alkali metals, Russian Chem. Rev. 40 (1971) 733–746.
70. F. J. Salzano, S. Aronson, Some experimental observations in caesium-graphite system, J. Inor. Nucl. Chem. 26 (1964) 1456–1458.

71. L. B. Ebert, Intercalation compounds of graphite, *Annu. Rev. Mater. Sci.* 6 (1976) 181–211.

Table 1. The Maxwellian closed-form calculated and experimental parameters of H₂, D₂, H₂⁺ and D₂⁺.

Parameter	Calculated	Experimental
H ₂ Bond Energy	4.478 eV	4.478 eV
D ₂ Bond Energy	4.556 eV	4.556 eV
H ₂ ⁺ Bond Energy	2.654 eV	2.651 eV
D ₂ ⁺ Bond Energy	2.696 eV	2.691 eV
H ₂ Total Energy	31.677 eV	31.675 eV
D ₂ Total Energy	31.760 eV	31.760 eV
H ₂ Ionization Energy	15.425 eV	15.426 eV
D ₂ Ionization Energy	15.463 eV	15.466 eV
H ₂ ⁺ Ionization Energy	16.253 eV	16.250 eV
D ₂ ⁺ Ionization Energy	16.299 eV	16.294 eV
H ₂ ⁺ Magnetic Moment	$9.274 \times 10^{-24} \text{ JT}^{-1} (\mu_B)$	$9.274 \times 10^{-24} \text{ JT}^{-1} (\mu_B)$
Absolute H ₂ Gas-Phase NMR Shift	-28.0 ppm	-28.0 ppm
H ₂ Internuclear Distance ^a	0.748 Å $\sqrt{2}a_o$	0.741 Å
D ₂ Internuclear Distance ^a	0.748 Å $\sqrt{2}a_o$	0.741 Å
H ₂ ⁺ Internuclear Distance	1.058 Å $2a_o$	1.06 Å
D ₂ ⁺ Internuclear Distance ^a	1.058 Å $2a_o$	1.0559 Å
H ₂ Vibrational Energy	0.517 eV	0.516 eV
D ₂ Vibrational Energy	0.371 eV	0.371 eV
H ₂ $\omega_e x_e$	120.4 cm ⁻¹	121.33 cm ⁻¹
D ₂ $\omega_e x_e$	60.93 cm ⁻¹	61.82 cm ⁻¹
H ₂ ⁺ Vibrational Energy	0.270 eV	0.271 eV
D ₂ ⁺ Vibrational Energy	0.193 eV	0.196 eV
H ₂ J=1 to J=0 Rotational Energy ^a	0.0148 eV	0.01509 eV
D ₂ J=1 to J=0 Rotational Energy ^a	0.00741 eV	0.00755 eV
H ₂ ⁺ J=1 to J=0 Rotational Energy	0.00740 eV	0.00739 eV
D ₂ ⁺ J=1 to J=0 Rotational Energy ^a	0.00370 eV	0.003723 eV

^a Not corrected for the slight reduction in internuclear distance due to \bar{E}_{osc} .

Table 2. The reactants, and their purity, vendors, and conditions of preparation.

Compound	Chemical Name and Description	Supplier	Preparation
KH	Potassium hydride, 30-35% w/w in mineral oil	Alfa Aesar	washed with anhydrous hexane and dried under vacuum at room temperature for 4 h
NaH	Sodium hydride, 57-63% oil dispersion	Alfa Aesar	washed with anhydrous hexane and dried under vacuum at room temperature for 4 h
Ca	Calcium granules, redistilled, -16 mesh, 99.5% (metals basis)	Alfa Aesar	as received
Li	Li granules, 1- 6 mm (0.04 – 0.2 in.), 99% (metal basis)	Alfa Aesar	as received
Mg	Magnesium powder, -325 mesh, 99.8%	Alfa Aesar	as received
Activated Carbon	Carbon powder, activated, Ash 4% max	Alfa Aesar	dried at 750 °C under vacuum for 48 h
Carbon black	Carbon black, acetylene, 50% compressed, 99.9+% (metals basis), S.A. 75m ² /g, Bulk density 5.9-6.4lbs/ft ³	Alfa Aesar	dried at 650 °C under vacuum for 28 h
Pd/C	Palladium on carbon, extent of labeling: 1 wt. % loading, 4-8 mesh	Sigma Aldrich	dried at 400 °C under vacuum for 72 h
TiC	Titanium carbide, 30-50 nm APS powder, S.A. 35-45m ² /g, MP ca 3140 °C; BP 4820 °C	Alfa Aesar	dried at 500 °C under vacuum for 48 h
TiCN	Titanium carbonitride (TiC _{0.7} N _{0.3}), Purity: > 97%, APS: 50-80 nm, SSA: 15 - 25 m ² /g, Color: black, Morphology: spherical & polyhedral	Accumet Materials Co.	dried at 400 °C under vacuum for 48 h
Ti ₃ SiC ₂	Titanium silicon carbide, maxthal 312, ceramic powder, d50: 3 μm	3-ONE-2 LLC	dried at 400 °C under vacuum for 48 h
WC nano	Tungsten carbide (WC), Purity: 99.5%, APS: 90-300 nm, SSA: 1.1 m ² /g, Morphology: nearly spherical	Accumet Materials Co.	dried at 400 °C under vacuum for 48 h
YC ₂	Yttrium Carbide, 12 mm pcs & smaller typ, 99.5%, MP ~ 2400 °C	Cerac, Inc.	dried at 200 °C under vacuum for 24 h, ground to a fine powder
LiBr	Lithium bromide, anhydrous, 99% min, 500 g, FW 86.85; MP 550 °C	Alfa Aesar	dried at 400 °C under vacuum for 24 h
LiCl	Lithium chloride, ACS, 99% min, 500 g, MP 605 °C	Alfa Aesar	dried at 400 °C under vacuum for 48 h
MgF ₂	Magnesium fluoride, 99.5% (metals basis excluding Ca & Na), Ca+Na <1%, -200 Mesh Powder, FW 62.30; MP 1261 °C	Alfa Aesar	dried at 300 °C under vacuum for 24 h
MgCl ₂	Magnesium chloride, anhydrous, 99%, MP 714 °C	Alfa Aesar	dried at 300 °C under vacuum for 24 h
MgBr ₂	Magnesium bromide, off-white powder, anhydrous, 98%, MP 700 °C	Strem	as received
MgI ₂	Magnesium iodide, <i>ultra dry</i> , 99.996% (metals basis), powder, ampule under argon, MP 637 °C dec	Alfa Aesar	as received
CaF ₂	Calcium fluoride, reagent grade, 97%, powder, MP 1403 °C	Alfa Aesar	dried at 300 °C under vacuum for 24 h
CaCl ₂	Calcium chloride, anhydrous, ACS, 96.0% min, powder, packaged under argon, MP 782 °C	Alfa Aesar	dried at 300 °C under vacuum for 24 h

CaBr ₂	Calcium bromide, anhydrous, 99.5%, -80 mesh powder, MP 742 °C	Alfa Aesar	dried at 750 °C under vacuum for 12 h
CaI ₂	Calcium iodide, anhydrous, 99.5% (metals basis), -20 mesh powder, MP 784 °C	Alfa Aesar	dried at 300 °C under vacuum for 24 h
SrF ₂	Strontium fluoride, 99% min, powder, MP 1473 °C	Alfa Aesar	dried at 300 °C under vacuum for 24 h
SrCl ₂	Strontium chloride, anhydrous, 99.5%, powder, MP 873 °C	Alfa Aesar	dried at 300 °C under vacuum for 24 h
SrBr ₂	Strontium bromide, anhydrous, 99% (metals basis excluding Ba), Ba 0.1% max, granular; MP 643 °C	Alfa Aesar	dried at 200 °C under vacuum for 24 h
SrI ₂	Strontium iodide, powder, anhydrous, 99.99% (metals basis), MP 515 °C	Alfa Aesar	dried at 753 °C under vacuum for 12 h
BaF ₂	Barium fluoride, 99%, -40 Mesh Powder, MP 1353 °C	Alfa Aesar	dried at 300 °C under vacuum for 24 h
BaCl ₂	Barium chloride, anhydrous, min 98+%, white powder, MP 963 °C	Strem	dried at 300 °C under vacuum for 24 h
BaBr ₂	Barium bromide, anhydrous, 99%, granular, MP 850 °C	Alfa Aesar	dried at 300 °C under vacuum for 24 h
BaI ₂	Barium iodide, anhydrous, min. 97%, MP 740 °C	Strem	dried at 798 °C under vacuum for 42 h

MP = melting point, BP=boiling point, SA=surface area, SSA=specific surface area, dec=decomposes

Table 3. The maximum energetic reaction, XRD results, experimental net energy E_{net} , energy released per mole ΔH of alkaline earth halide, lithium halide, or per mole of H for hydrino reactions given by Eqs. (19–22) and (28–30), respectively, calculated theoretical maximum energy E_{mt} for conventional chemistry [66–68] ($-\Delta H$), excess heat from the hydrino reaction E_{ex} , maximum temperature of run T , and energy gain G of hydrino catalyst systems.

Reactants	Maximum Energetic Reaction	XRD Results	E_{net} (kJ)	ΔH	E_{mt} (kJ)	E_{ex}^a (kJ)	T (°C)	G^b
				$\frac{\text{kJ}}{\text{mole}}$				
8.3g KH + 5.0g Mg + 20.0g TiC + 3.1g MgF ₂	No exothermic reaction		10	200.0	0	10	389	Inf.
8.3g KH + 5.0g Mg + 20.0g YC ₂ + 3.1g MgF ₂	No exothermic reaction	YC ₂ 13.3 ± 0.3% (710 Å) KMgH ₃ 32.0 ± 0.6% (>1,000 Å) Mg 16.0 ± 0.4% (>1,000 Å) KMgH ₃ 20.1 ± 0.4% (412 Å) MgF ₂ 6.8 ± 0.4% (>1,000 Å) K ₂ MgH ₄ 11.8 ± 0.4% (>1,000 Å)	11	220	0	11	406	Inf.
8.3g KH + 5.0g Mg + 20.0g TiC + 4.75g MgCl ₂	MgCl ₂ (c) + 2KH(c) → 2KCl(c) + MgH ₂ (c)		20.9	418	9.6	11.3	390	2.2
8.3g KH + 5.0g Mg + 20.0g YC ₂ + 4.75g MgCl ₂	MgCl ₂ (c) + 2KH(c) → 2KCl(c) + MgH ₂ (c)	KCl 29.6 ± 0.5% (429 Å) KMgH ₃ 39.3 ± 0.7% (>1,000 Å) Mg 18.1 ± 0.4% (>1,000 Å) YC ₂ 13.0 ± 0.4% (704 Å)	23.4	467	9.6	13.8	408	2.4
8.3g KH + 5.0g Mg + 20.0g TiC + 9.2g MgBr ₂	MgBr ₂ (c) + 2KH(c) → 2KBr(c) + MgH ₂ (c)	KBr 22.3 ± 0.1% (627 Å) KMgH ₃ 10.1 ± 0.1% (620 Å) K ₂ MgH ₄ 2.4 ± 0.1% (285 Å) Mg 13.3 ± 0.2% (>1,000 Å) TiC 51.9 ± 0.3% (510 Å)	25.1	502	11.2	13.9	357	2.2
8.3g KH + 5.0g Mg + 20.0g TiC + 13.9g MgI ₂	MgI ₂ (c) + 2KH(c) → 2KI(c) + MgH ₂ (c)		20	400	12.6	7.4	380	1.6

Reactants	Maximum Energetic Reaction	XRD Results	E_{net} (kJ)	ΔH	E_{mt} (kJ)	E_{ex}^a (kJ)	T (°C)	G^b
				$\frac{\text{kJ}}{\text{mole}}$				
8.3g KH + 5.0g Mg + 20.0g TiC + 3.9g CaF ₂	No exothermic reaction	CaF ₂ 3.2 ± 0.1% (>1,000 Å) K 2.0 ± 0.1% (467 Å) KH 4.2 ± 0.2% (536 Å) K ₂ MgH ₄ 8.0 ± 0.2% (>1,000 Å) KMgH ₃ 11.9 ± 0.4% (106 Å) K ₂ Ti F ₆ 2.6 ± 0.1% (640 Å) Mg 10.0 ± 0.3% (>1,000 Å) MgF ₂ 3.9 ± 0.2% (628 Å) TiC 54.2 ± 0.6% (315 Å)	9	189	0	9	461	Inf.
8.3g KH + 5.0g Mg + 20.0g YC ₂ + 3.9 CaF ₂	No exothermic reaction		9.2	184	0	9.2	370	Inf.
8.3g KH + 5.0g Mg + 20.0g TiC + 5.55g CaCl ₂	CaCl ₂ (c) + 2KH(c) → 2KCl(c) + CaH ₂ (c)	CaCl ₂ 4.2 ± 0.2% (613 Å) CaH ₂ 2.8 ± 0.1% (485 Å) KCl 5.6 ± 0.2% (167 Å) Mg 16.8 ± 0.7% (553 Å) TiC 61.1 ± 0.8% (323 Å) MgCl ₂ 8.4 ± 0.3% (906 Å) Ti 1.1 ± 0.1% (385 Å)	13.6	270	7.2	6.4	359	1.9
8.3g KH + 5.0g Mg + 20.0g YC ₂ + 5.55g CaCl ₂	CaCl ₂ (c) + 2KH(c) → 2KCl(c) + CaH ₂ (c)		14.5	290	7.2	7.3	367	2.0
8.3g KH + 5.0g Mg + 20.0g TiC + 10.0g CaBr ₂	CaBr ₂ (c) + 2KH(c) → 2KBr(c) + CaH ₂ (c)	KBr 19.9 ± 0.2% (467 Å) Mg 11.5 ± 0.3% (>1,000 Å) CaH ₂ 4.3 ± 0.1% (>1,000 Å) MgH ₂ 1.5 ± 0.2% (>1,000 Å) TiC 54.2 ± 0.5% (279 Å) K ₂ MgH ₄ 5.6 ± 0.3% (183 Å) KMgH ₃ 3.0 ± 0.2% (444 Å)	22	440	8.6	13.4	396	2.6
8.3g KH + 5.0g Mg + 20.0g TiC + 14.7g CaI ₂	CaI ₂ (c) + 2KH(c) → 2KI(c) + CaH ₂ (c)		9.8	196.2	9.4	0.4	363	1.0

Reactants	Maximum Energetic Reaction	XRD Results	E_{net} (kJ)	ΔH	E_{mt} (kJ)	E_{ex}^a (kJ)	T (°C)	G^b
				$\frac{\text{kJ}}{\text{mole}}$				
8.3g KH + 5.0g Mg + 20.0g TiC + 6.3g SrF ₂	No exothermic reaction		4.8	95.8	0	4.8	343	Inf.
8.3g KH + 5.0g Mg + 20.0g TiC + 7.95g SrCl ₂	SrCl ₂ (c) + 2KH(c) → 2KCl(c) + SrH ₂ (c)	K 4.0 ± 0.2% (>1,000 Å) KCl 15.2 ± 0.2% (253 Å) KH 0.7 ± 0.1% (>1,000 Å) Mg 14.8 ± 0.3% (>1,000 Å) TiH ₂ 0.4 ± 0.1% (>1,000 Å) TiC 64.9 ± 0.6% (325 Å)	13.1	262	5.4	7.7	382	2.4
8.3g KH + 5.0g Mg + 20.0g TiC + 4.76g SrCl ₂	SrCl ₂ (c) + 2KH(c) → 2KCl(c) + SrH ₂ (c)	K 2.3 ± 0.1% (349 Å) KCl 5.9 ± 0.2% (326 Å) KH 2.4 ± 0.2% (323 Å) KMgH ₃ 4.5 ± 0.2% (264 Å) K ₂ MgH ₄ 5.9 ± 0.3% (227 Å) Mg 10.6 ± 0.2% (>1,000 Å) SrH ₂ 3.1 ± 0.1% (474 Å) TiC 65.3 ± 0.5% (238 Å)	11.6	387	3.3	8.3	537	3.5
8.3g KH + 5.0g Mg + 20.0g YC ₂ + 7.95g SrCl ₂	SrCl ₂ (c) + 2KH(c) → 2KCl(c) + SrH ₂ (c)		9	180	5.4	3.6	540	1.6
8.3g KH + 5.0g Mg + 20.0g TiC + 12.4g SrBr ₂	SrBr ₂ (c) + 2KH(c) → 2KBr(c) + SrH ₂ (c)	KBr 20.1 ± 0.2% (452 Å) KMgH ₃ 3.9 ± 0.1% (346 Å) Mg 14.9 ± 0.4% (662 Å) SrH ₂ 6.5 ± 0.1% (472 Å) TiC 54.6 ± 0.5% (303 Å)	17.7	355	6.7	11	400	2.6
4.98g KH + 3.0g Mg + 12.0g YC ₂ + 7.44g SrBr ₂	SrBr ₂ (c) + 2KH(c) → 2KBr(c) + SrH ₂ (c)	KBr 29.5 ± 0.3% (409 Å) KMgH ₃ 16.0 ± 0.3% (461 Å) Mg 18.0 ± 0.4% (565 Å) YC ₂ 28.4 ± 0.3% (549 Å) SrH ₂ 8.1 ± 0.2% (555 Å)	10	333	4.0	6	485	2.5

Reactants	Maximum Energetic Reaction	XRD Results	E_{net} (kJ)	ΔH	E_{mt} (kJ)	E_{ex}^a (kJ)	T (°C)	G^b
				$\frac{\text{kJ}}{\text{mole}}$				
8.3g KH + 5.0g Mg + 20.0g TiC + 17.1g SrI ₂	SrI ₂ (c) + 2KH(c) → 2KI(c) + SrH ₂ (c)	KI 19.8 ± 0.2% (519 Å) KMgH ₃ 6.6 ± 0.3% (312 Å) Mg 15.3 ± 0.4% (>1,000 Å) SrH ₂ 6.9 ± 0.2% (581 Å) TiC 51.4 ± 0.6% (354 Å)	26	520	8.1	17.9	424	3.2
8.3g KH + 5.0g Mg + 20.0g TiC + 8.75g BaF ₂	No exothermic reaction	BaF ₂ 10.6 ± 0.1% (555 Å) BaH ₂ 3.2 ± 0.1% (780 Å) KH 4.4 ± 0.2% (350 Å) Mg 13.4 ± 0.4% (922 Å) TiC 57.6 ± 0.6% (318 Å) K ₂ MgH ₄ 8.5 ± 0.3% (513 Å) TiF ₃ 2.1 ± 0.3% (435 Å)	13	260	0	13	365	Inf.
8.3g KH + 5.0g Mg + 20.0g TiC + 10.4g BaCl ₂	BaCl ₂ (c) + 2KH(c) → 2KCl(c) + BaH ₂ (c)	BaCl ₂ 0.6 ± 0.1% (>1,000 Å) K 6.7 ± 0.3% (337 Å) KH 2.6 ± 0.2% (534 Å) KMgH ₃ 4.1 ± 0.2% (940 Å) K ₂ MgH ₄ 15.4 ± 0.4% (339 Å) Mg 9.3 ± 0.4% (>1,000 Å) TiC 61.4 ± 0.8% (279 Å)	13.8	276	4.1	9.7	545	3.4
8.3g KH + 5.0g Mg + 20.0g YC ₂ + 10.4g BaCl ₂	BaCl ₂ (c) + 2KH(c) → 2KCl(c) + BaH ₂ (c)	BaCl ₂ 11.5 ± 0.2% (701 Å) BaH ₂ 1.0 ± 0.1% (506 Å) BaHCl 2.8 ± 0.2% (297 Å) KH 10.5 ± 0.2% (>1,000 Å) KMgH ₃ 14.5 ± 0.3% (996 Å) K ₂ MgH ₄ 15.4 ± 0.3% (884 Å) Mg 26.1 ± 0.4% (>1,000 Å) YC ₂ 18.2 ± 0.2% (642 Å)	11.4	228	4.1	7.3	362	2.8

Reactants	Maximum Energetic Reaction	XRD Results	E_{net} (kJ)	ΔH	E_{mt} (kJ)	E_{ex}^a (kJ)	T (°C)	G^b
				$\frac{\text{kJ}}{\text{mole}}$				
8.3g KH + 5.0g Mg + 20.0g TiC + 14.85g BaBr ₂	BaBr ₂ (c) + 2KH(c) → 2KBr(c) + BaH ₂ (c)	Ba 0.7 ± 0.1% (>1,000 Å) BaBr ₂ 19.1 ± 0.4% (614 Å) BaHBr 1.3 ± 0.1% (617 Å) KBr 2.5 ± 0.2% (>1,000 Å) KH 1.9 ± 0.2% (612 Å) KMgH ₃ 1.9 ± 0.1% (>1,000 Å) Mg 8.6 ± 0.5% (>1,000 Å) TiC 64.0 ± 0.9% (378 Å)	13.0	260	4.7	8.3	334	2.8
8.3g KH + 5.0g Mg + 20.0g YC ₂ + 14.85g BaBr ₂	BaBr ₂ (c) + 2KH(c) → 2KBr(c) + BaH ₂ (c)	BaBr ₂ 23.3 ± 1.0% (902 Å) BaHBr 2.9 ± 0.4% (>1,000 Å) Ba ₂ Mg ₁₇ 5.5 ± 0.5% (>1,000 Å) KBr 9.0 ± 0.6% (212 Å) KMgH ₃ 14.5 ± 0.8% (609 Å) Mg 19.9 ± 1.0% (979 Å) MgBr ₂ 4.3 ± 0.6% (232 Å) YC ₂ 20.6 ± 0.7% (767 Å)	17.2	343	4.7	12.5	396	3.7
8.3g KH + 5.0g Mg + 20.0g TiC + 19.55g BaI ₂	BaI ₂ (c) + 2KH(c) → 2KI(c) + BaH ₂ (c)	KH 6.2 ± 0.2% (478 Å) KI 3.8 ± 0.1% (485 Å) KMgH ₃ 7.2 ± 0.2% (>1,000 Å) K ₂ MgH ₄ 14.7 ± 0.3% (491 Å) Mg 6.3 ± 0.3% (>1,000 Å) TiC 61.8 ± 0.7% (329 Å)	11	220	5.9	5.1	424	1.9
8.3g KH + 5.0g Mg + 20.0g YC ₂ + 19.55g BaI ₂	BaI ₂ (c) + 2KH(c) → 2KI(c) + BaH ₂ (c)		27.6	553	5.9	21.7	411	4.7
8.3g KH + 5g Mg + 20g TiC + 2.13g LiCl	KH(c) + LiCl(c) → KCl(c) + LiH(c)	K 2.0 ± 0.1% (337 Å) KCl 4.3 ± 0.2% (258 Å) KH 1.2 ± 0.2% (262 Å) KMgH ₃ 1.5 ± 0.2% (252 Å) K ₂ MgH ₄ 14.1 ± 0.2% (346 Å) Mg 8.9 ± 0.3% (792 Å) TiC 68.0 ± 0.5% (248 Å)	9.7	194	3.0	6.7	478	3.2

Reactants	Maximum Energetic Reaction	XRD Results	E_{net} (kJ)	ΔH	E_{mt} (kJ)	E_{ex}^a (kJ)	T (°C)	G^b
				$\frac{\text{kJ}}{\text{mole}}$				
8.3g KH + 5g Mg + 20g TiC + 2.13g LiCl	KH(c) + LiCl(c) → KCl(c) + LiH(c)		10.3	206	3.0	7.3	711	3.4
8.3g KH + 5g Mg + 20g TiC + 2.13g LiCl	KH(c) + LiCl(c) → KCl(c) + LiH(c)		11	220	3.0	8	710	3.7
4.98g KH + 3g Mg + 12g TiCN + 1.3g LiCl	KH(c) + LiCl(c) → KCl(c) + LiH(c)	KCl 14.7 ± 0.2% (306 Å) K ₂ MgH ₄ 10.0 ± 0.2% (287 Å) KMgH ₃ 2.8 ± 0.1% (436 Å) Mg 13.3 ± 0.3% (521 Å) Ti(C,N) 59.2 ± 0.5% (2481 Å)	5	167	1.8	3.2	555	2.8
8.3g KH + 5g Mg + 20g WC + 2.13g LiCl	KH(c) + LiCl(c) → KCl(c) + LiH(c)	WC 49.4 ± 0.6% (163 Å) KCl 32.9 ± 0.5% (210 Å) K ₂ MgH ₄ 17.7 ± 0.5% (983 Å)	11.2	224	3.0	8.2	716	3.7
8.3g KH + 5g Mg + 20g WC + 2.13g LiCl	KH(c) + LiCl(c) → KCl(c) + LiH(c)		8.3	166	3.0	5.3	632	2.8
8.3g KH + 5g Mg + 20g Ti ₃ SiC ₂ + 2.13g LiCl	KH(c) + LiCl(c) → KCl(c) + LiH(c)	K 2.8 ± 0.2% (381 Å) KCl 5.8 ± 0.3% (254 Å) KMgH ₃ 2.1 ± 0.2% (318 Å) K ₂ MgH ₄ 11.0 ± 0.4% (209 Å) Mg 12.2 ± 0.4% (316 Å) Ti ₃ SiC ₂ 57.4 ± 0.8% (227 Å) TiC 8.7 ± 0.3% (285 Å)	13.3	265	3.0	10.3	712	4.4
5g NaH + 5g Mg + 20g TiC + 2.13g LiCl	NaH(c) + LiCl(c) → NaCl(c) + LiH(c)		10.5	210	1.8	8.7	699	5.8

Reactants	Maximum Energetic Reaction	XRD Results	E_{net} (kJ)	ΔH	E_{mt} (kJ)	E_{ex}^a (kJ)	T (°C)	G^b
				$\frac{\text{kJ}}{\text{mole}}$				
5g NaH + 5g Mg + 20g TiC + 2.13g LiCl	NaH(c) + LiCl(c) → NaCl(c) + LiH(c)	Mg 12.7 ± 0.3% (>1,000 Å) Na 7.9 ± 0.5% (49 Å) NaCl 8.0 ± 0.3% (245 Å) NaH 3.4 ± 0.4% (496 Å) NaMgH ₃ 0.9 ± 0.1% (>1,000 Å) Ti 0.3 ± 0.1% (764 Å) TiC 66.8 ± 0.7% (251 Å)	10	200	1.8	8.2	720	5.5
5g NaH + 5g Mg + 20g TiC + 2.13g LiCl	NaH(c) + LiCl(c) → NaCl(c) + LiH(c)		10.7	214	1.8	8.9	686	5.9
5g NaH + 5g Mg + 20g TiCN + 2.13g LiCl	NaH(c) + LiCl(c) → NaCl(c) + LiH(c)	Mg 14.6 ± 0.3% (953 Å) Na 4.6 ± 0.3% (65 Å) NaCl 7.0 ± 0.2% (539 Å) NaH 4.8 ± 0.4% (415 Å) Ti 1.1 ± 0.1% (448 Å) Ti(C, N) 67.9 ± 0.7% (227 Å)	11.8	236	1.8	10	716	6.6
5g NaH + 5g Mg + 20g WC + 2.13g LiCl	NaH(c) + LiCl(c) → NaCl(c) + LiH(c)	LiC 12.0 ± 0.5% (233 Å) Mg 23.3 ± 0.7% (274 Å) NaCl 25.0 ± 0.7% (273 Å) NaMgH ₃ 5.8 ± 0.4% (223 Å) WC 33.9 ± 0.8% (161 Å)	11.2	224	1.8	9.4	710	6.2
5g NaH + 5g Mg + 20g YC ₂ + 2.13g LiCl	NaH(c) + LiCl(c) → NaCl(c) + LiH(c)	(Li,Mg) ₂ Cl ₄ 0.8 ± 0.3% (>1,000 Å) Mg 33.7 ± 1.1% (350 Å) MgCl ₂ 11.9 ± 0.3% (171 Å) Na 17.0 ± 0.3% (115 Å) NaCl 6.8 ± 0.1% (426 Å) NaMgCl ₃ 5.8 ± 0.3% (270 Å) YC ₂ 22.6 ± 0.6% (508 Å) YH ₂ 1.4 ± 0.1% (638 Å)	7	140	1.8	5.2	570	3.8
8.3g KH + 5g Mg + 20g YC ₂ + 4.35g LiBr	KH(c) + LiBr(c) → KBr(c) + LiH(c)		11	220	3.8	7.2	568	2.9

Reactants	Maximum Energetic Reaction	XRD Results	E_{net} (kJ)	ΔH	E_{mt} (kJ)	E_{ex}^a (kJ)	T (°C)	G^b
				$\frac{\text{kJ}}{\text{mole}}$				
8.3g KH + 5g Mg + 20g YC ₂ + 4.35g LiBr	KH(c) + LiBr(c) → KBr(c) + LiH(c)		17	340	3.8	13.2	490	4.5
5g NaH + 5g Mg + 20g YC ₂ + 4.35g LiBr	NaH(c) + LiBr(c) → NaBr(c) + LiH(c)		10	200	2.2	7.8	573	4.5
5g NaH + 5g Mg + 20g YC ₂ + 4.35g LiBr	NaH(c) + LiBr(c) → NaBr(c) + LiH(c)		12	240	2.2	9.8	445	5.4
8.3g KH + 5g Mg + 2.13g LiCl	KH(c) + LiCl(c) → KCl(c) + LiH(c)		9.3	186	3.0	6.3	739	3.1
5g NaH + 5g Mg + 2.13g LiCl	NaH(c) + LiCl(c) → NaCl(c) + LiH(c)		7.9	158	1.8	6.1	710	4.4
8.3g KH + 12g Pd/C	KH(c) + 8C(s) → C ₈ KH _{0.14} (s) + 0.43H ₂ (g)	C KH Pd	11.2	54.0	1.3	9.9	571	8.6
3g NaH + 3g Mg + 6g Pd/C	No exothermic reaction	Mg NaH Mg ₈₅ Pd ₁₄ NaMgH ₃ Pd ₃ H ₄	8.6	69.8	0	8.6	501	Inf.
42.0g KH + 25.0g Mg + 100.0g Carbon Black	KH(c) + 8C(s) → C ₈ KH _{0.14} (s) + 0.43H ₂ (g)		26	24.8	10.5	15.5	495	2.5

Reactants	Maximum Energetic Reaction	XRD Results	E_{net} (kJ)	ΔH	E_{mt} (kJ)	E_{ex}^a (kJ)	T (°C)	G^b	
				$\frac{\text{kJ}}{\text{mole}}$					
8.3g KH + 5g Mg + 20g TiC	No exothermic reaction	K KH KMgH ₃ K ₂ MgH ₄ Mg MgH ₂ TiC	2.5 ± 0.1% (390 Å) 5.5 ± 0.2% (383 Å) 3.6 ± 0.2% (462 Å) 13.1 ± 0.3% (304 Å) 16.8 ± 1.3% (555 Å) 3.0 ± 0.2% (>1,000 Å) 55.5 ± 0.5% (267 Å)	5.8	30.0	0	5.8	489	Inf.
8.3g KH + 5g Mg + 20g TiC	No exothermic reaction			5.2	25.1	0	5.2	596	Inf.
8.3g KH + 5g Mg + 20g TiC	No exothermic reaction			6.6	31.8	0	6.6	575	Inf.
5g NaH + 5g Mg + 20g TiC	No exothermic reaction			7.0	33.6	0	7.0	522	Inf.
5g NaH + 5g Mg + 20g TiC	No exothermic reaction	Mg NaMgH ₃ NaH Na Ti TiC	3.9 ± 0.1% (>1,000 Å) 0.8 ± 0.1% (496 Å) 5.8 ± 0.2% (565 Å) 2.4 ± 0.2% (114 Å) 0.9 ± 0.1% (141 Å) 86.2 ± 0.5% (252 Å)	6.6	31.7	0	6.6	524	Inf.
5g NaH + 5g Mg + 20g TiC	No exothermic reaction			6.0	28.8	0	6.0	556	Inf.
8.3g KH + 20g TiC + 0.35g Li	KH(c) + Li(c) → LiH(c) + K(c)			8.9	43.0	1.6	7.3	552	5.6
8.3g KH + 20g TiC + 0.35g Li	KH(c) + Li(c) → LiH(c) + K(c)			6.5	31.4	1.6	4.9	542	4.1
5g NaH + 20g TiC + 0.35g Li	NaH(c) + Li(c) → LiH(c) + Na(c)			6.2	29.8	1.7	4.5	545	3.6

Reactants	Maximum Energetic Reaction	XRD Results	E_{net} (kJ)	ΔH	E_{mt} (kJ)	E_{ex}^a (kJ)	T (°C)	G^b
				$\frac{\text{kJ}}{\text{mole}}$				
8.3g KH + 5g Mg + 20g TiC + 0.35g Li	$\text{KH(c)} + \text{Li(c)} \rightarrow \text{LiH(c)} + \text{K(c)}$		12.0	58.0	1.6	10.4	540	7.5
8.3g KH + 5g Mg + 20g TiC + 0.35g Li	$\text{KH(c)} + \text{Li(c)} \rightarrow \text{LiH(c)} + \text{K(c)}$		14.8	71.5	1.6	13.2	564	9.3
5g NaH + 5g Mg + 20g TiC + 0.35g Li	$\text{NaH(c)} + \text{Li(c)} \rightarrow \text{LiH(c)} + \text{Na(c)}$		11.1	53.3	1.7	9.4	590	6.5
5g NaH + 20g TiC	No exothermic reaction	Na $7.4 \pm 0.3\%$ (36 Å) NaH $19.4 \pm 0.3\%$ (308 Å) TiC $73.2 \pm 0.5\%$ (178 Å)	5.8	27.8	0	5.8	572	Inf.
5g NaH + 20g TiC	No exothermic reaction	NaH $19.0 \pm 0.3\%$ (361 Å) TiC $81.0 \pm 0.6\%$ (210 Å)	4.3	20.6	0	4.3	581	Inf.
5g NaH + 20g TiC	No exothermic reaction		4.7	22.6	0	4.7	596	Inf.

^a Difference of experimental net energy and calculated theoretical maximum ($E_{net} - E_{mt}$).

^b Ratio of the experimental net energy and calculated theoretical maximum (E_{net} / E_{mt}).

Table 4. Reactant amounts, temperature, duration, and XRD results of regeneration reactions demonstrating that the halide hydride exchange reaction is thermally reversible. Oxide was from XRD holder air leak.

Regeneration Reactants	XRD (wt %)	Notes
4.8g KF + 1.0g Mg, SS crucible, 750 °C, vacuum, 1h	KF 0.8 ± 0.1% (>1,000 Å) KMgF ₃ 93.0 ± 0.8% (>1,000 Å) K ₂ MgF ₄ 3.9 ± 0.2% (>1,000 Å) MgF ₂ 2.3 ± 0.2% (556 Å)	3.4g grey crystalline product.
3.5g KF + 1.2g Ca, SS crucible, 870 °C, vacuum, 2 h,	KCaF ₃ 86.8 ± 1.3% (>1,000 Å) CaF ₂ 11.6 ± 0.2% (>1,000Å) KF 1.4 ± 0.2% (203 Å) K 0.2 ± 0.1% (>1,000Å)	2.4g product.
6.0g (0.080 mole) KCl + 1.6g (0.040 mole) Ca in SS crucible, 550 °C, vacuum, 1h	KCl 20.5 ± 0.3% (564 Å) KCaCl ₃ 79.5 ± 1.0% (514 Å)	
6.0g (0.080 mole) KCl + 1.6g (0.040 mole) Ca in SS crucible, 750 °C, vacuum, 1h	CaCl ₂ 15.5 ± 0.3% (414 Å) KCl 70.1 ± 1.5% (983 Å) KCaCl ₃ 14.4 ± 0.5% (379 Å)	1.3g white crystalline product
0.84g Ca + 5.0g KBr, 730 °C, vacuum, 3h	CaBr ₂ 87.0 ± 1.1% (814 Å) Ca 4.5 ± 0.1% (308 Å) CaBrH 1.8 ± 0.2% (904 Å) KOH 6.7 ± 0.1% (922 Å)	4.0g white solid, 1.5g K deposit
2.35g Sr + 4.00g KCl, 800 °C, vacuum, 3h	SrCl ₂ ~50% (969 Å) KSr ₂ Cl ₅ ~37% (>1,000 Å) KCl ~ 1% (320 Å) Sr ₄ OCl ₆ ~12% (681 Å)	
4.0g KCl + 2.35g Sr, SS tube, 750 °C, vacuum, 3h	KSr ₂ Cl ₅ 86% (>1,000 Å) Sr ₄ OCl ₆ 11% (>1,000 Å) SrO 3% (>1,000 Å)	2.1g K, ~2.0g white solid.
1.3g Sr + 3.5g KBr, 780 °C, 30 min, 1 atm Ar, 780 °C, vacuum, 30 min	Major: SrBr ₂ (307 Å) Trace: Unknown (234 Å)	2.8g light purple powder.
7.1g(0.060 mol) KBr + 2.6g (0.030 mole) Sr, SS crucible, 780 °C, 1 atm Ar, 0.5h, followed by vacuum, 40 min	Major: SrBr ₂ (>1,000 Å) Minor: (KBr)(SrBr ₂) ₂ (689 Å)	5.0g light purple crystals
7.1g (0.060 mol) KBr + 2.6g (0.030 mole) Sr, SS crucible, 780 °C, vacuum, 0.5 hour	SrBr ₂ 92.3 ± 1.4% (>1,000 Å) SrO 2.1 ± 0.1% (736 Å) Sr ₄ OBr ₆ 5.6 ± 0.3% (332 Å)	2.0 g, purple colored crystalline product
2.5g Sr + 8.0g KI, 690 °C, vacuum, 3h	KSr ₂ I ₅ ~72% (476 Å) SrI ₂ ~28% (473 Å)	
3.68g Ba + 4.00g KCl, 780 °C, 1 atm Ar, 30 min, 780 °C, followed by vacuum, 30 min	BaCl ₂ 81.5 ± 1.2% (446 Å) BaCl ₂ (H ₂ O) ₂ 15.9 ± 0.2% (912 Å) KCl 1.5 ± 0.2% (>1,000 Å) K 1.1 ± 0.2% (>1,000 Å)	2.8g white powder.

2.2g Ba + 4.1g KBr + 1.0g Mg, 3.65g SS wool, SS vessel, Ar was bubbled through the chemical (10 sccm)	Major: BaBr ₂ (741 Å) Unknown (300 Å) Minor: KBr (305 Å)	1.5g product was collected.
2.2g Ba + 4.0g KBr + 1.0g Mg + 1.0g TiC, 750 °C, vacuum, 2h	Major: Unknown (>1,000 Å) BaBr ₂ (698 Å) Minor: TiC (379 Å) Ba ₄ OBr ₆ (548 Å)	Significant K deposit, 5.5g black/grey powder collected in SS crucible.
2.2g Ba + 4.1g KBr + 1.5g TiC, 750 °C, vacuum, 2h	BaBr ₂ 16.4 ± 0.6% (332 Å) Ba ₄ OBr ₆ 23.4 ± 0.4% (610 Å) KBr 42.5 ± 0.6% (794 Å) TiC 17.7 ± 0.6% (414 Å)	3.0g sample collected
2.3g Ba + 4g KBr, 750 °C, vacuum, 1h	Major: BaBr ₂ (450Å) Unknown (265 Å) Minor: Ba ₄ OBr ₆ (428 Å)	3.6g sample collected.
4.3g NaBr + 2.8g Ba, SS tube, 750 °C, vacuum, 1h	BaBr ₂ 59.4 ± 0.6% (519 Å) NaBr 40.6 ± 0.5% (407 Å)	2 g grey crystalline product
6.6g KI + 2.6g Ba, SS crucible, 750 °C, 1h, vacuum	BaI ₂ 53.5 ± 0.8% (729 Å) KI 8.0 ± 0.5% (468Å) Ba ₄ I ₆ O 33.1 ± 0.6% (>1,000 Å) K ₃ IO ₅ 5.4 ± 0.6% (>1,000 Å)	3.6g sample collected.
4.00g KCl + 0.426g LiH, 760 °C, 1 atm Ar, 30 min; followed by 720 °C, vacuum, 30 min	LiCl 87.5 ± 1.2% (611 Å) KCl 9.6 ± 0.4% (326 Å) LiCl(H ₂ O) 2.9 ± 0.2% (209Å)	1.8g grey powder
0.35g Li + 5.95g KBr, 730 °C, 30 min, 1 atm Ar; followed by 600 °C, vacuum, 30 min	LiBr 72.9 ± 0.4% (709Å) KBr 27.1 ± 0.2% (652 Å)	1.5 g product, white solid.
0.544g LiH + 4.00g NaCl, 780 °C, 1atm, Ar, 30 min; followed by 720 °C, vacuum, 30 min	LiCl 91.0 ± 1.1% (220 Å) NaCl 9.0 ± 0.2% (361 Å)	2.6g white powder, 1.2g Na.

Figure 1. A representative XRD of the reaction product of 8.3g KH + 5g Mg + 20g TiC + 2.13g LiCl showing K ($2.0 \pm 0.1\%$ (337 Å)); KCl ($4.3 \pm 0.2\%$ (258 Å)); KH ($1.2 \pm 0.2\%$ (262 Å)); KMgH₃ ($1.5 \pm 0.2\%$ (252 Å)); K₂MgH₄ ($14.1 \pm 0.2\%$ (346 Å)); Mg ($8.9 \pm 0.3\%$ (792 Å)); TiC ($68.0 \pm 0.5\%$ (248 Å)).

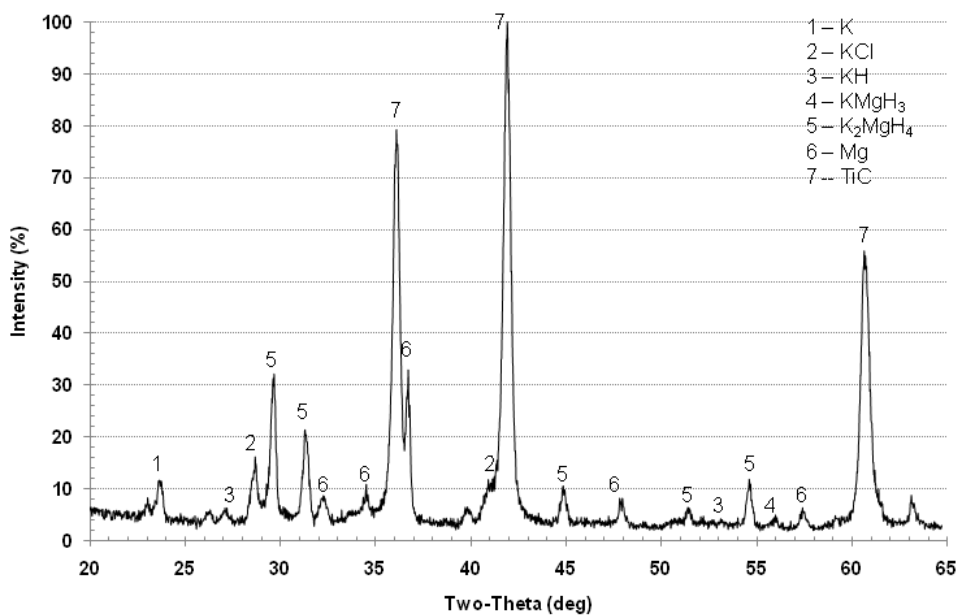


Figure 2. ^1H solution NMR recorded following DMF- d_7 solvent extraction of the products of a hydride-halide exchange system according to Eq. (19) comprising the reactants of 5g NaH + 5g Mg + 20g TiC + 12.4g SrBr₂ with the H₂(1/4) peak identified at about 1.26 ppm. The small peak at 2.2 ppm matches p = 2 in Eq. (18) corresponding to H₂(1/2).

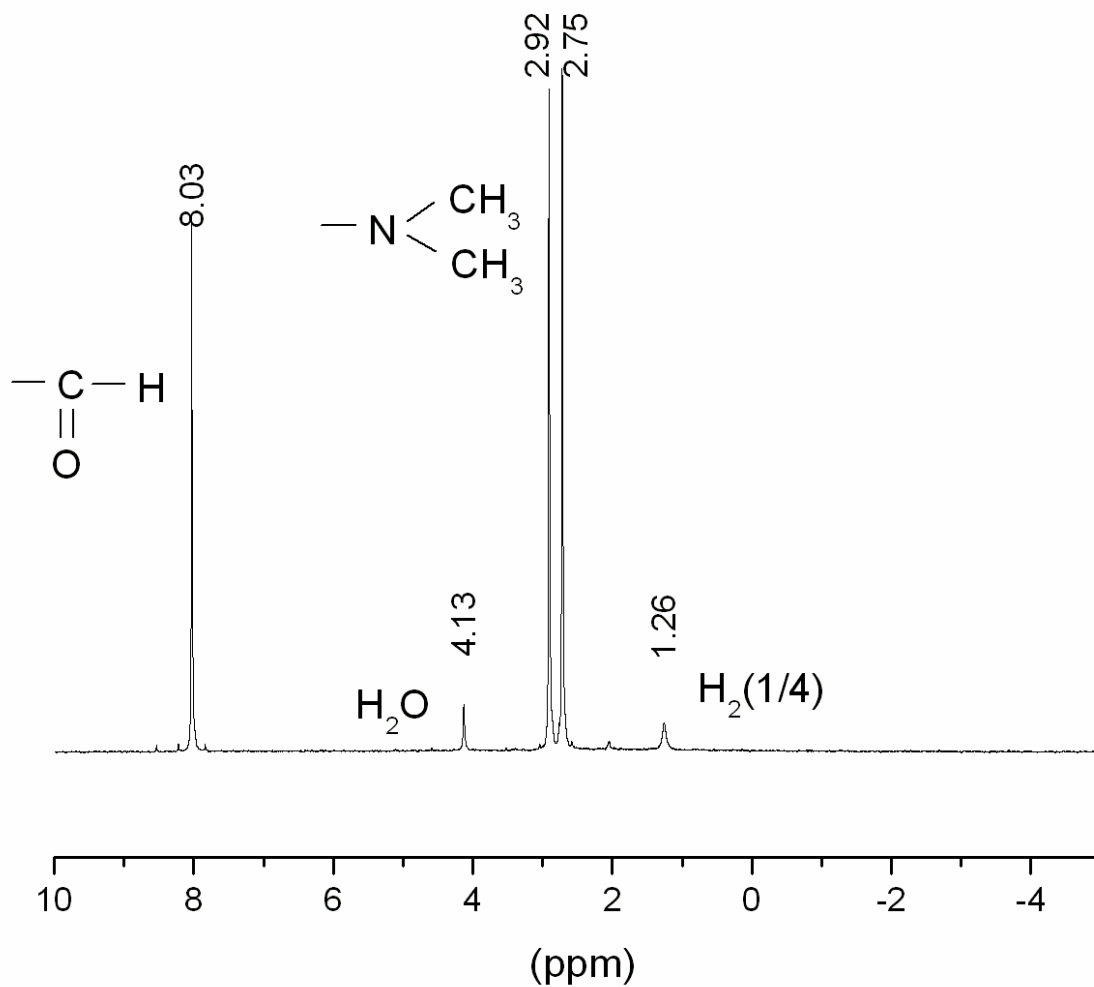


Figure 3. ^1H solution NMR recorded following DMF- d_7 solvent extraction of the products of a hydride-halide exchange system according to Eq. (19) comprising the reactants of 8.3g KH + 5g Mg + 20g TiC + 12.4g SrBr₂ with the H₂(1/4) peak identified at about 1.20 ppm.

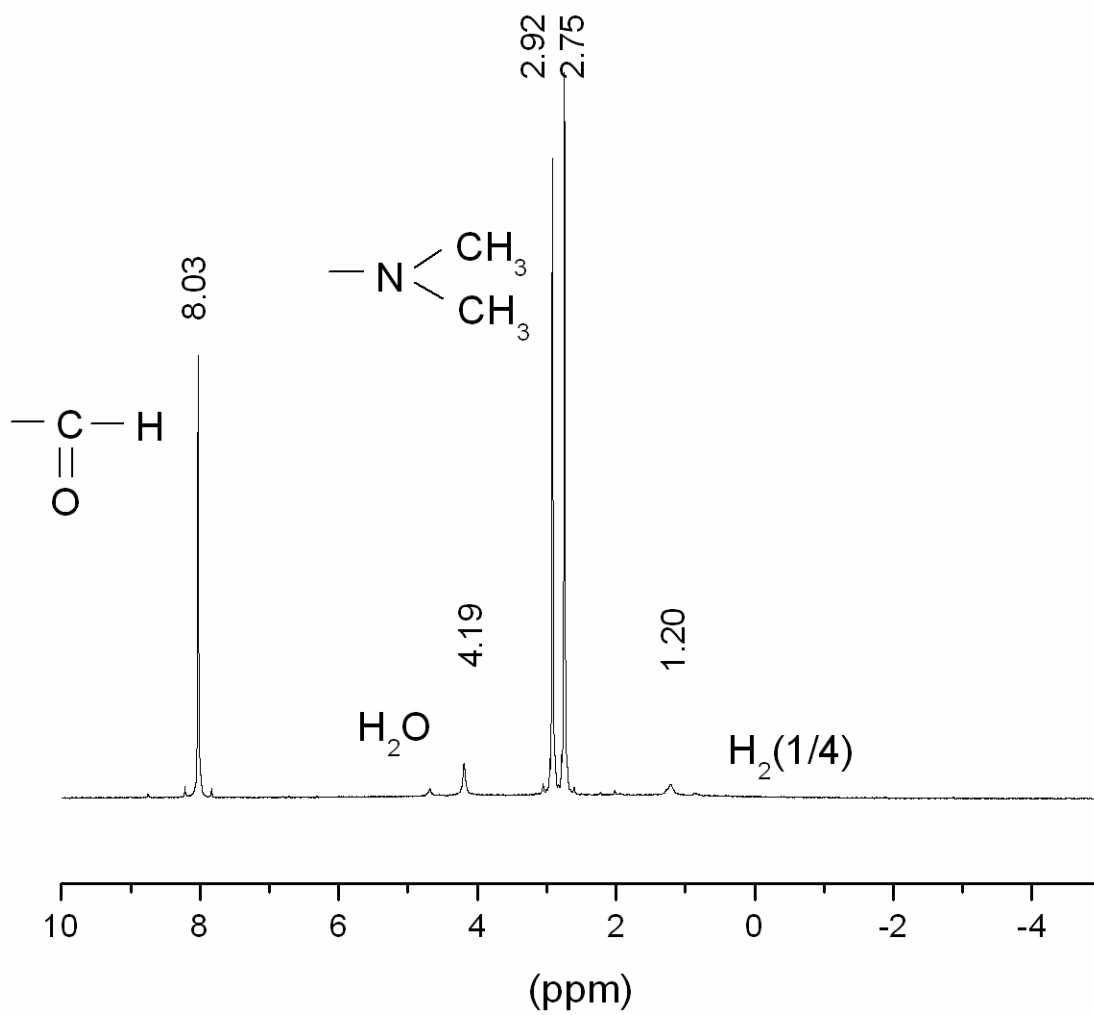


Figure 4. ^1H solution NMR recorded following DMF- d_7 solvent extraction of the products of a hydride-halide exchange system according to Eq. (20) comprising the reactants of 2g NaH + 2g Mg + 8g TiC + 0.85g LiCl with the $\text{H}_2(1/4)$ peak identified at about 1.21 ppm.

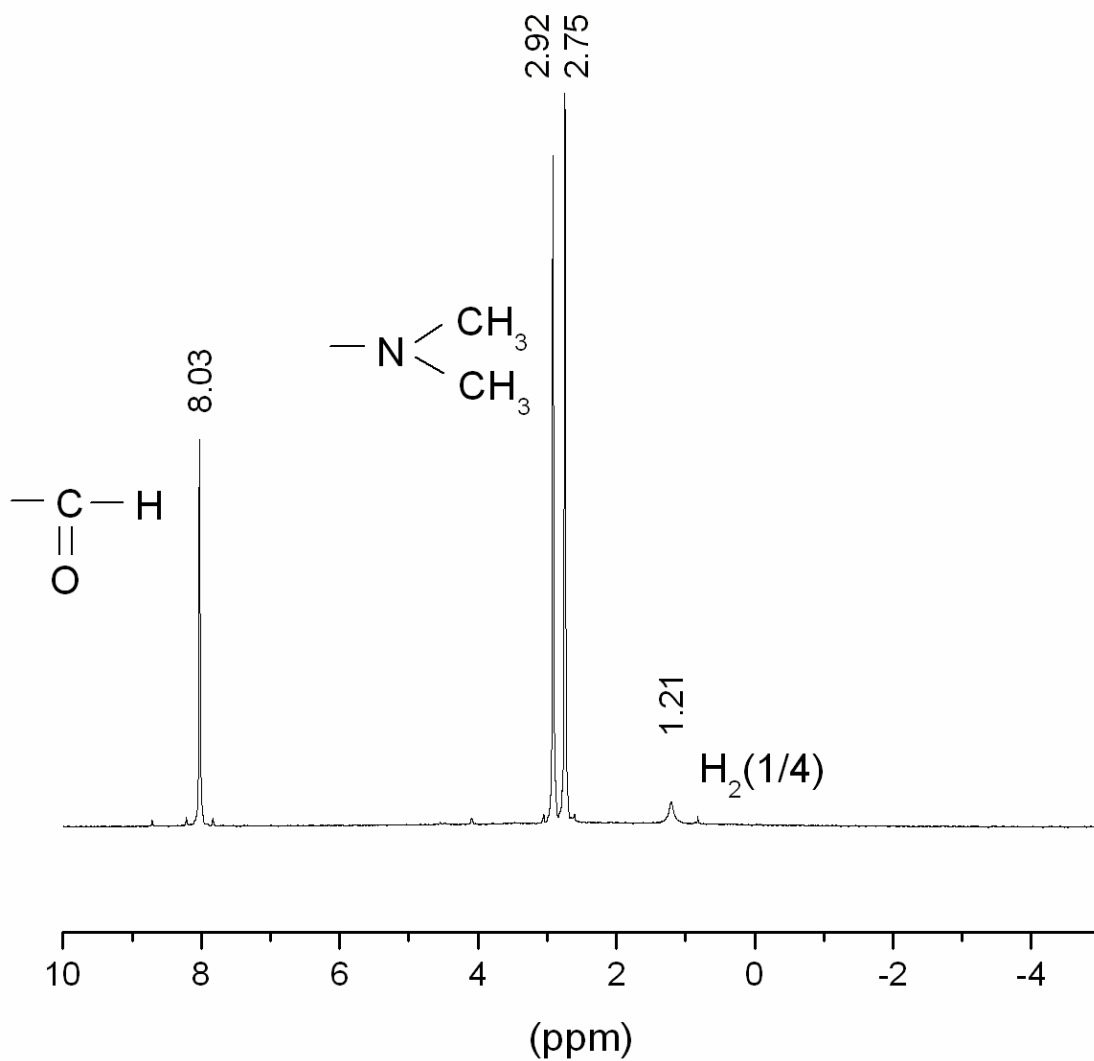


Figure 5. ^1H solution NMR recorded following DMF- d_7 solvent extraction of the products of a hydride-halide exchange system according to Eq. (20) comprising the reactants of 5g NaH + 5g Mg + 20g TiC + 4.34g LiBr with the $\text{H}_2(1/4)$ peak identified at about 1.26 ppm.

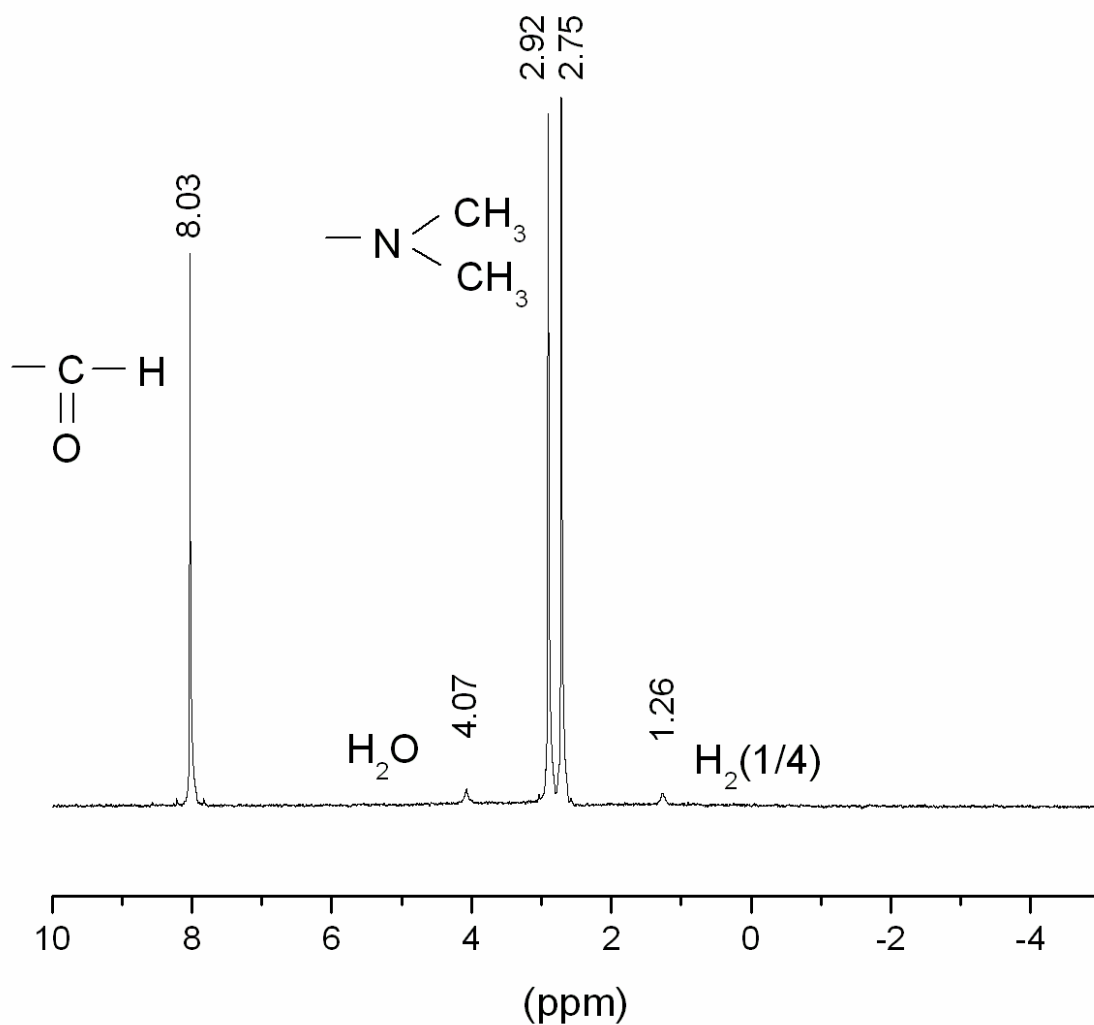


Figure 6. ^1H solution NMR recorded following DMF- d_7 solvent extraction of the products from the reactants of 4.98 g KH + 8 g Pd/C wherein carbon served as the oxidant according to Eq. (22) with the $\text{H}_2(1/4)$ peak identified at about 1.23 ppm.

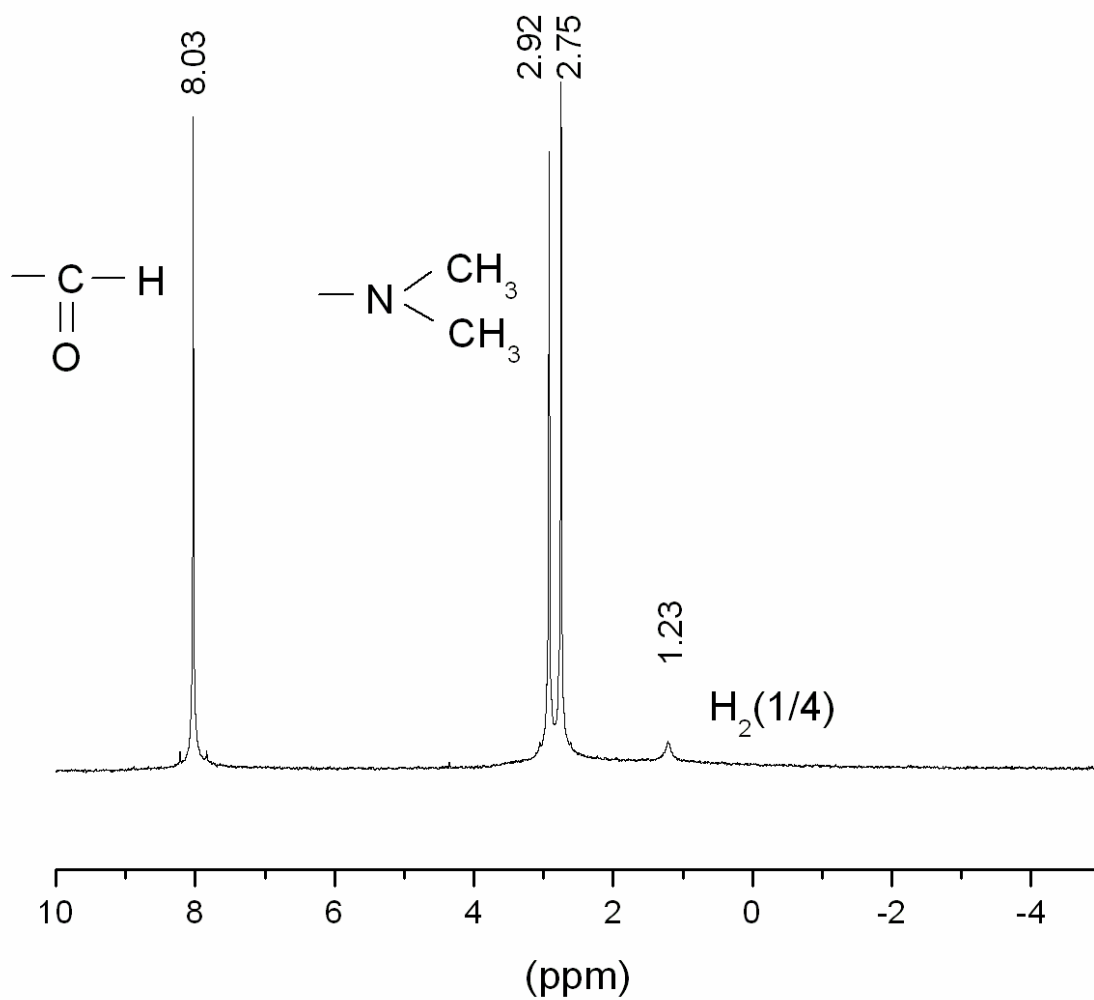


Figure 7. ^1H solution NMR recorded following DMF- d_7 solvent extraction of the products of a hydride exchange system according to Eq. (28) comprising the reactants of 2g NaH + 2g Mg + 8g TiC with the $\text{H}_2(1/4)$ peak identified at about 1.21 ppm. The small peak at 2.2 ppm matches $p = 2$ in Eq. (18) corresponding to $\text{H}_2(1/2)$.

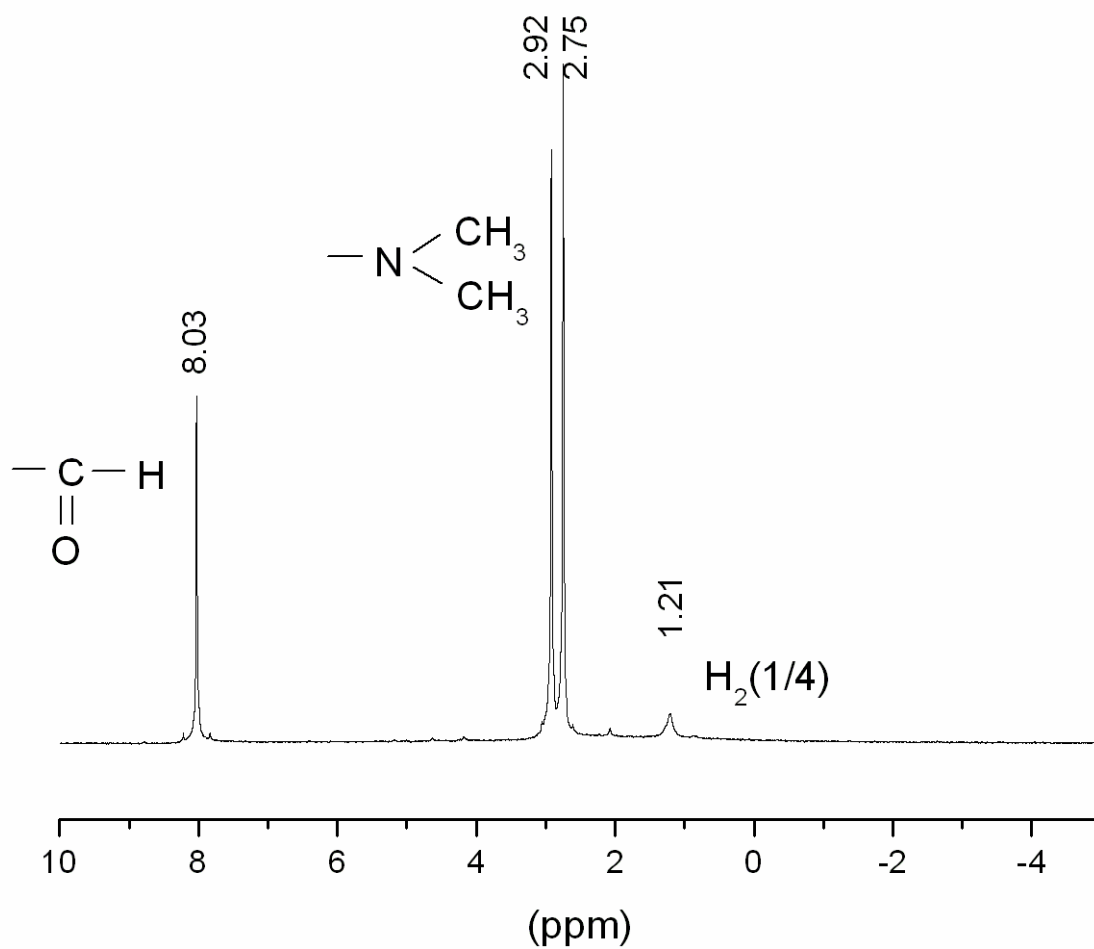


Figure 8. ^1H solution NMR recorded following DMF- d_7 solvent extraction of the products of a hydride exchange system according to Eq. (28) comprising the reactants of 8.3g KH + 5g Mg + 20g TiC with the $\text{H}_2(1/4)$ peak identified at about 1.21 ppm.

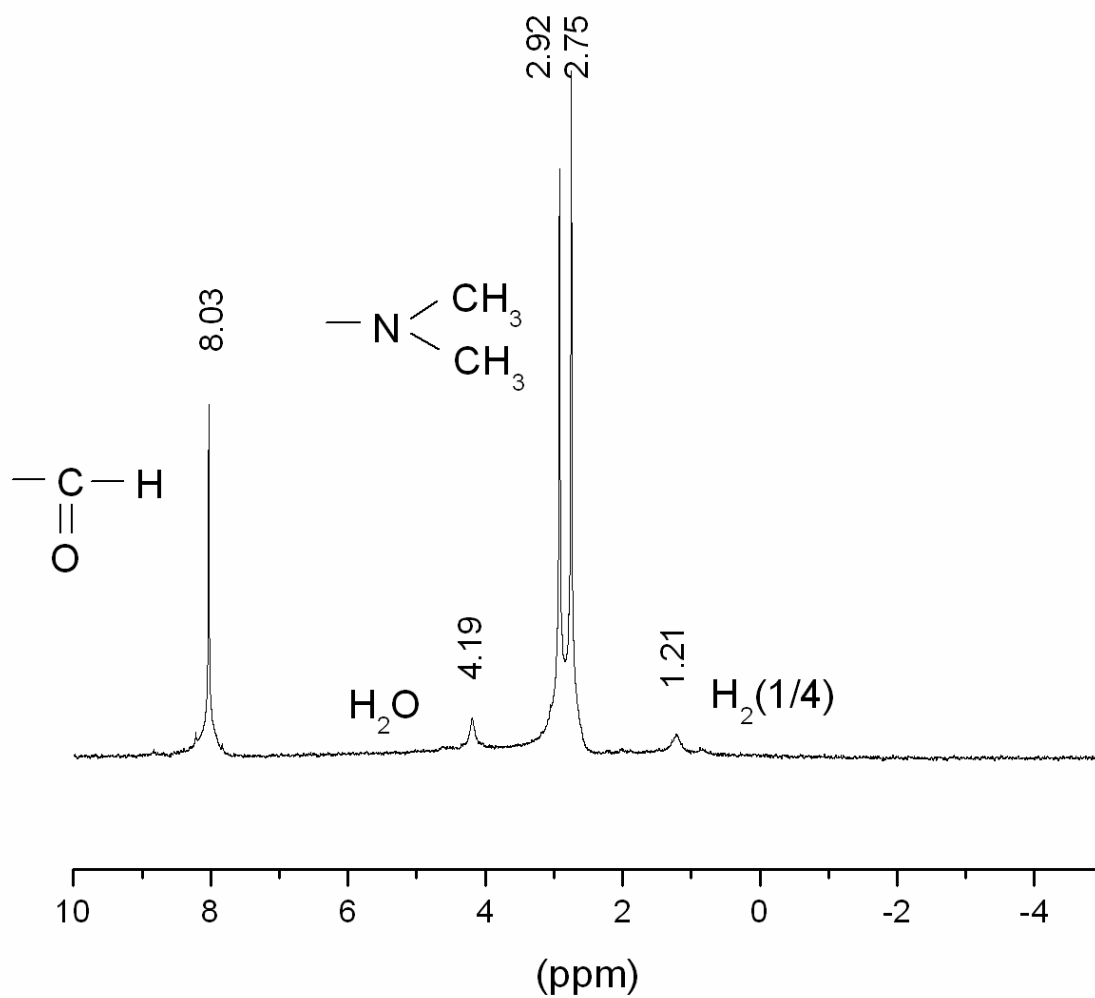


Figure 9. ^1H solution NMR recorded following DMF- d_7 solvent extraction of the products of a hydride exchange system according to Eq. (29) comprising the reactants of 8.3g KH + 20g TiC + 0.35g Li with the $\text{H}_2(1/4)$ peak identified at about 1.22 ppm.

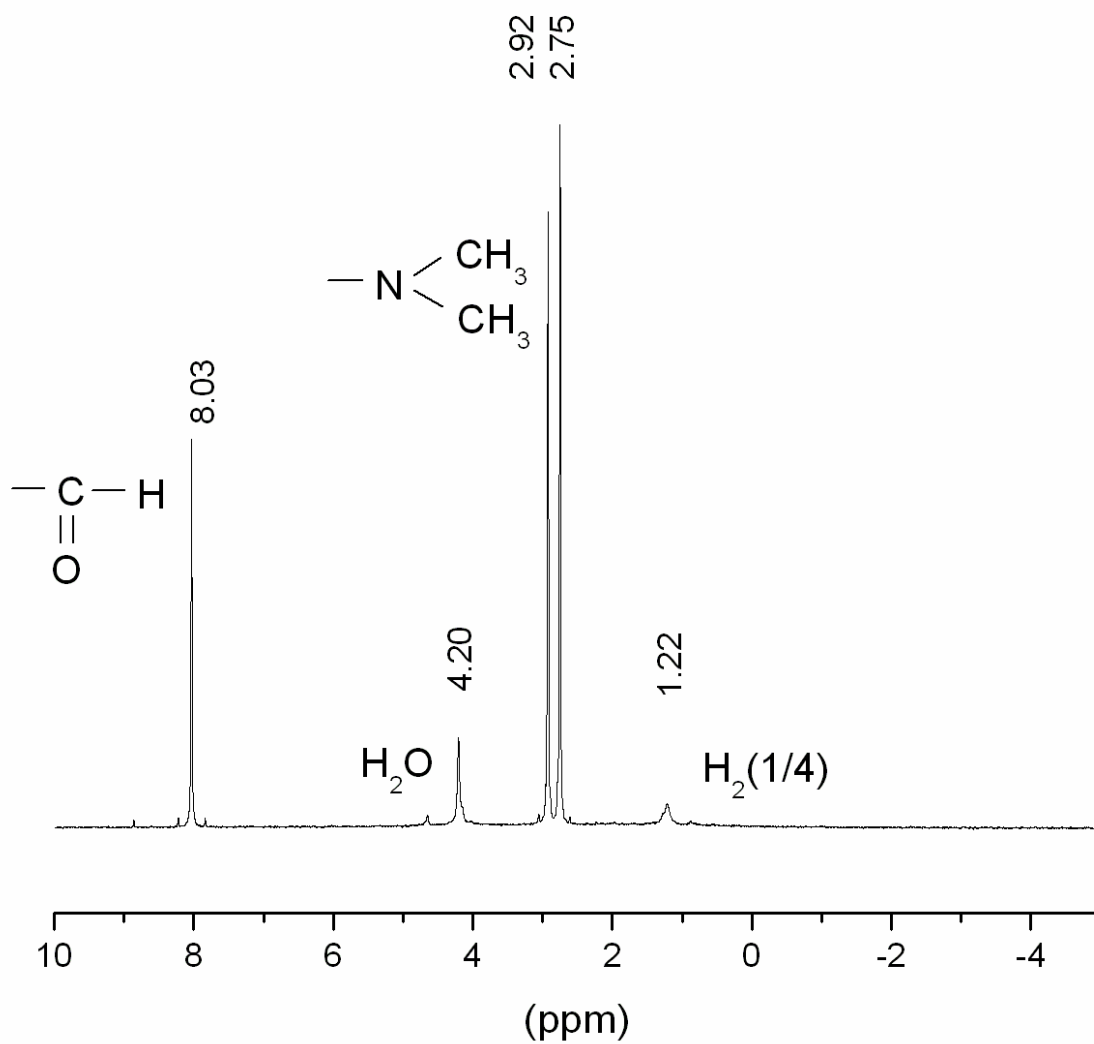


Figure 10. ^1H solution NMR recorded following DMF-d₇ solvent extraction of the products of a hydride exchange system according to Eq. (29) comprising the reactants of 5g NaH + 5g Mg + 2.13g LiCl with the $\text{H}_2(1/4)$ peak identified at about 1.21 ppm. The small peak at 2.2 ppm matches $p = 2$ in Eq. (18) corresponding to $\text{H}_2(1/2)$.

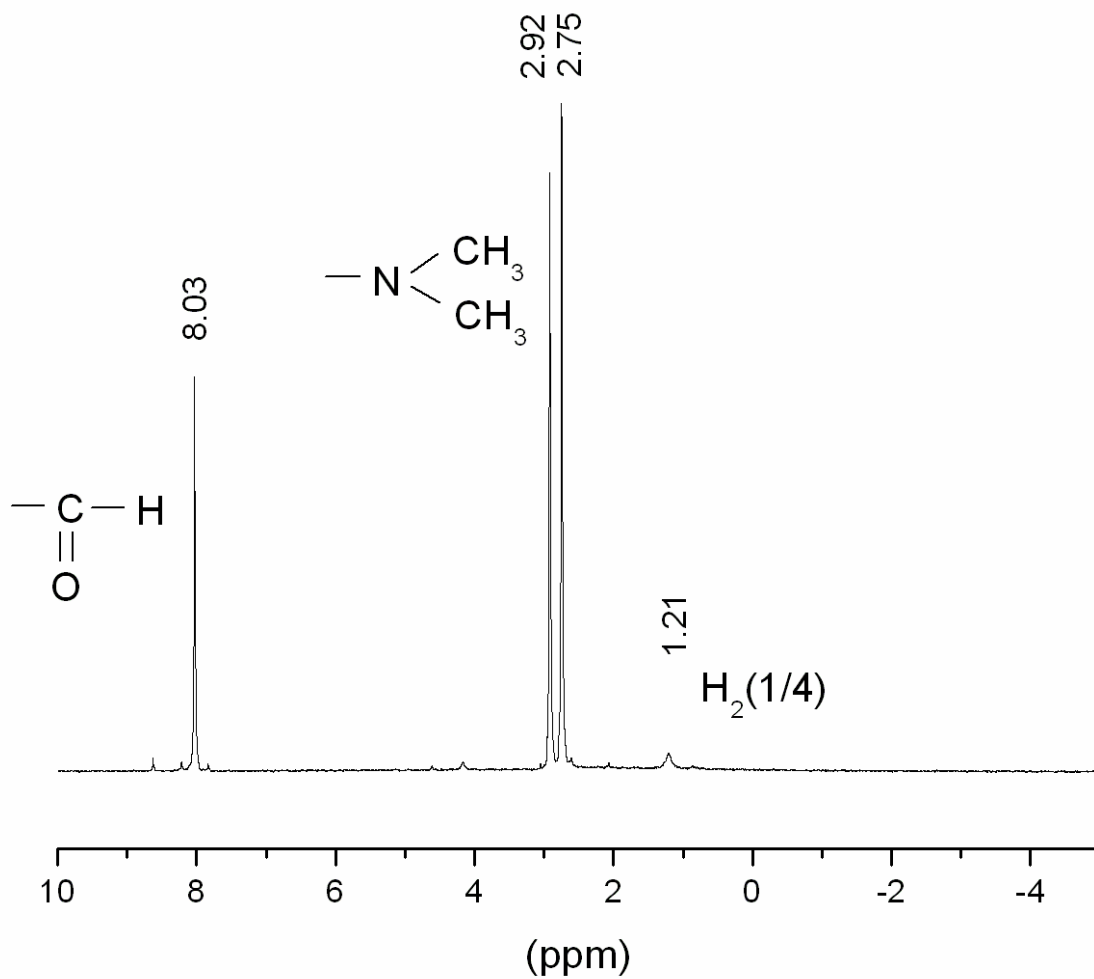


Figure 11. ^1H solution NMR recorded following DMF- d_7 solvent extraction of the products of a hydride exchange system according to Eq. (28) comprising the reactants of 3g NaH + 3g Mg + 12g Ti_3SiC_2 with the $\text{H}_2(1/4)$ peak identified at about 1.21 ppm.

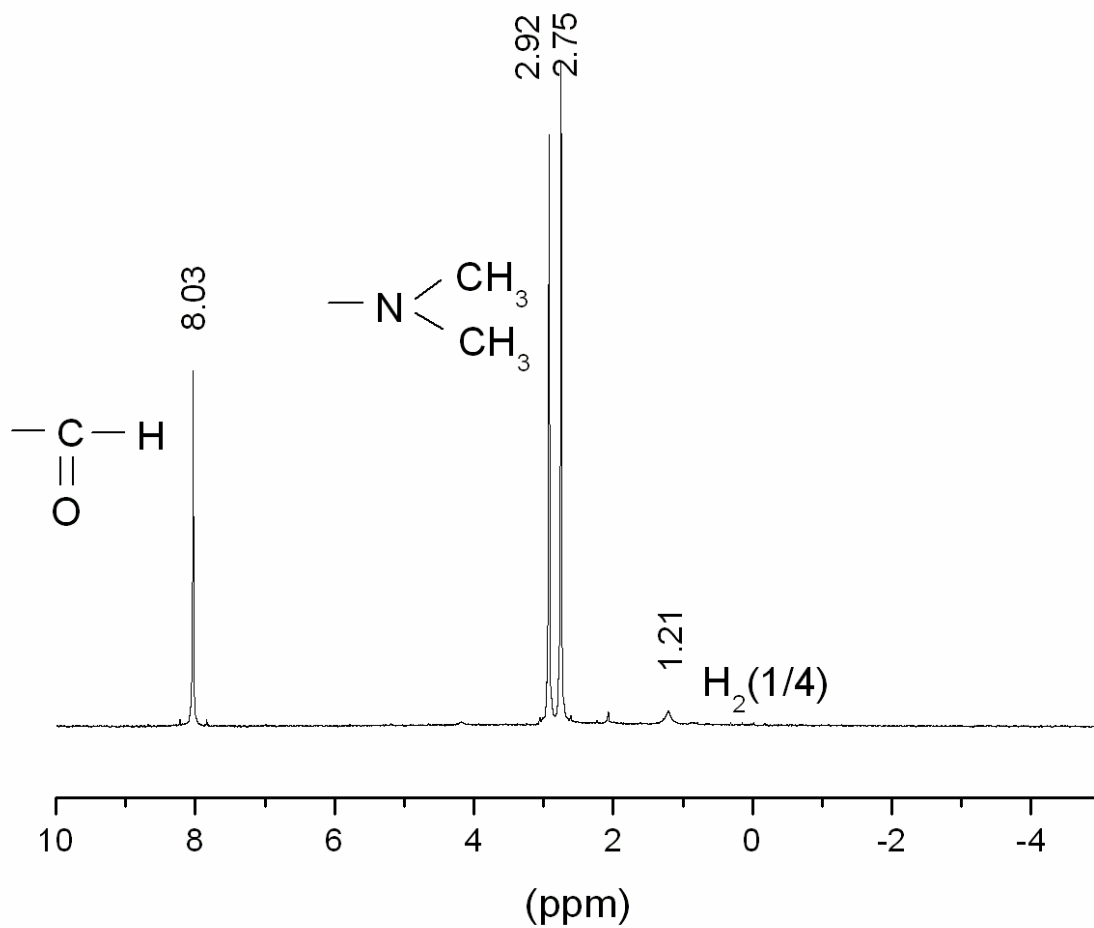


Figure 12. ^1H solution NMR recorded following DMF- d_7 solvent extraction of the products of a hydride exchange system according to Eq. (28) comprising the reactants of 3g NaH + 3g Mg + 6g Pd/C with the $\text{H}_2(1/4)$ peak identified at about 1.21 ppm.

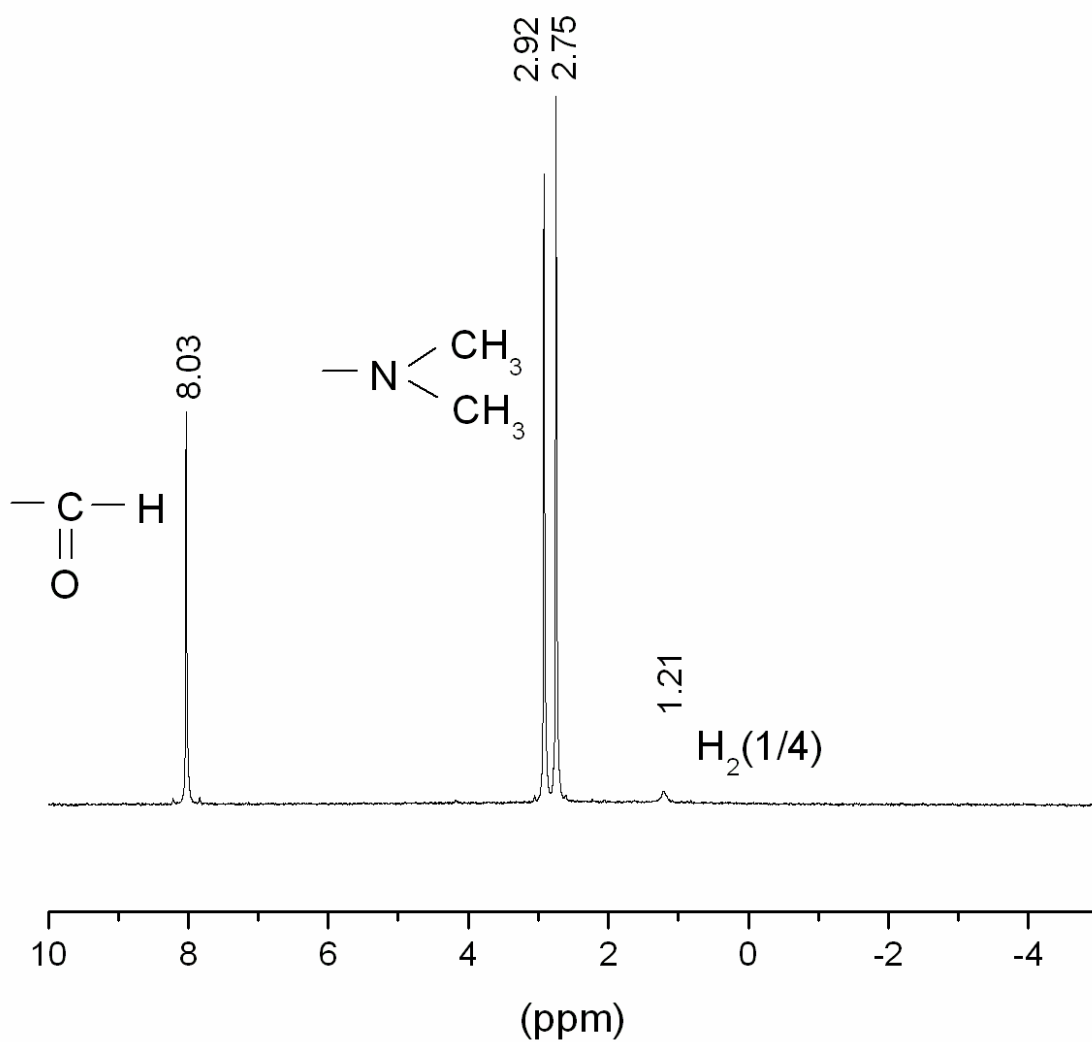


Figure 13. XPS survey spectrum ($E_B = 0$ eV to 1150 eV) recorded on the reaction product of 8.3g KH + 5g Mg + 20g TiC that produced an excess energy of 8.42 kJ.

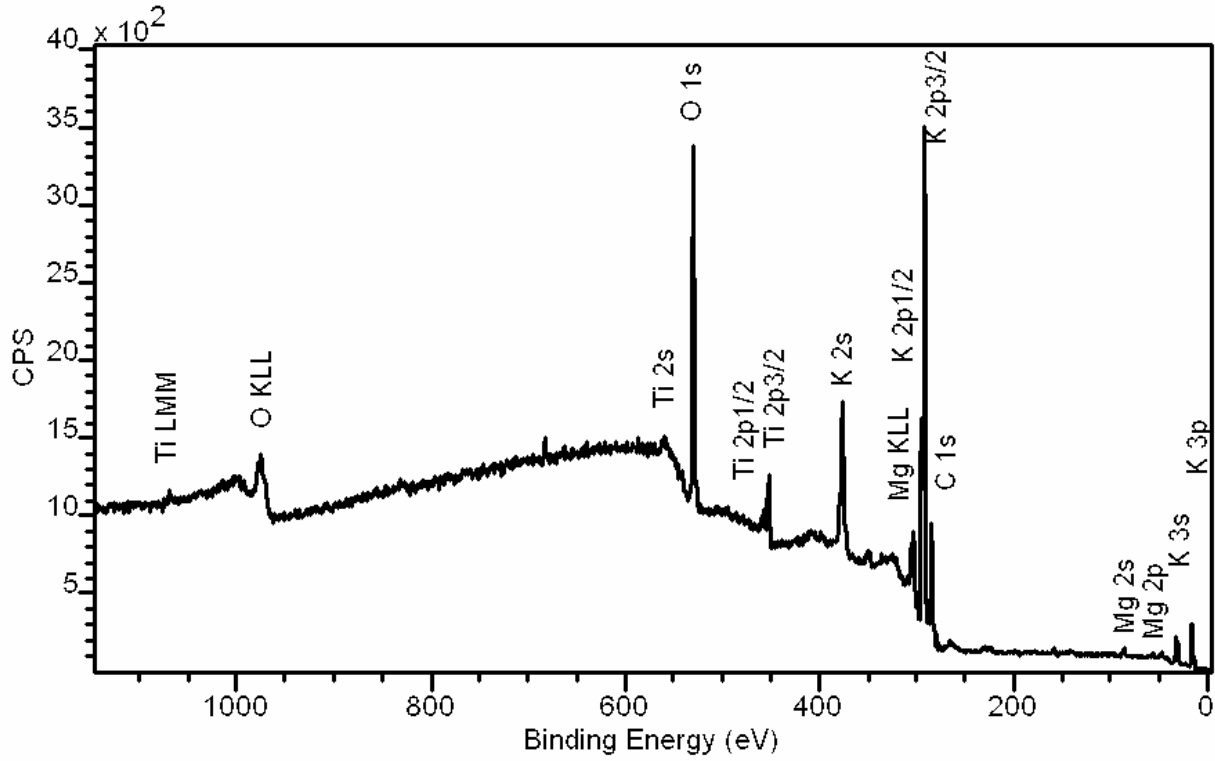


Figure 14. High resolution XPS spectrum ($E_B = 0$ eV to 120 eV) recorded on the reaction product of 8.3g KH + 5g Mg + 20g TiC that produced an excess energy of 8.42 kJ having peaks at 9.3 eV and 11.2 eV that could not be assigned to known elements and do not correspond to any other primary element peak but do match the H^- ($1/4$) $E_b = 11.2$ eV hydride ion in two chemical environments.

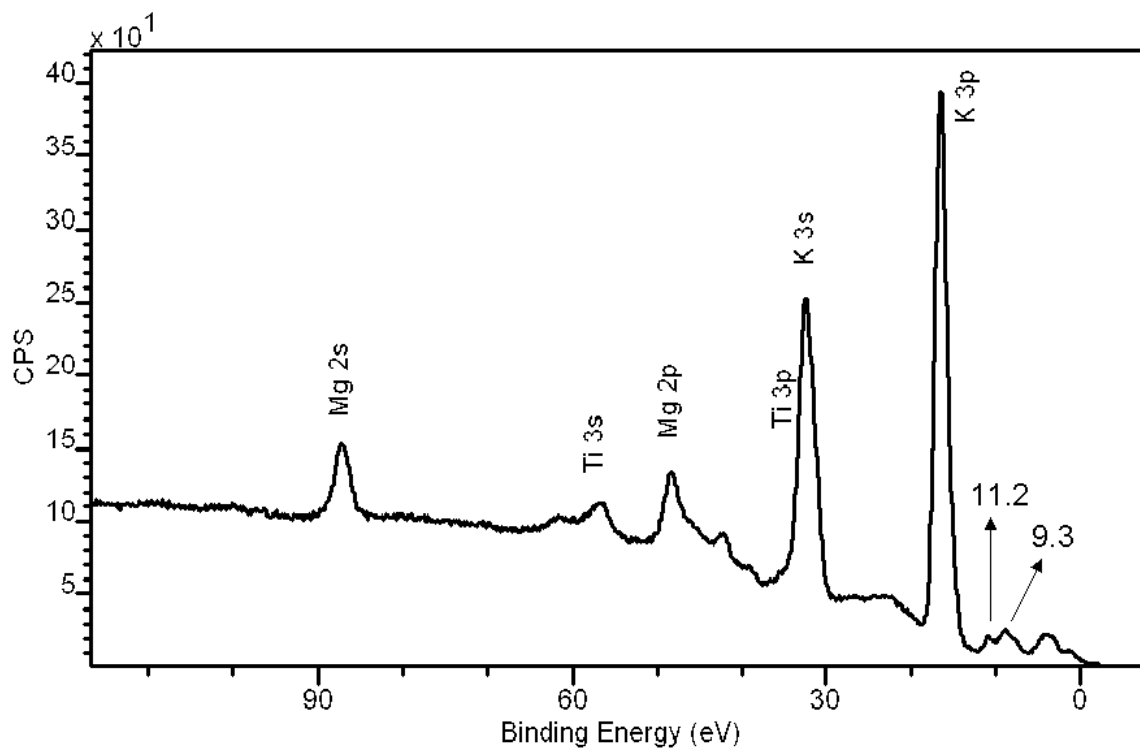


Figure 15. XPS survey spectrum ($E_B = 0$ eV to 1150 eV) recorded on the reaction product of 8.3g KH + 12g Pd/C that produced an excess energy of 9.94 kJ.

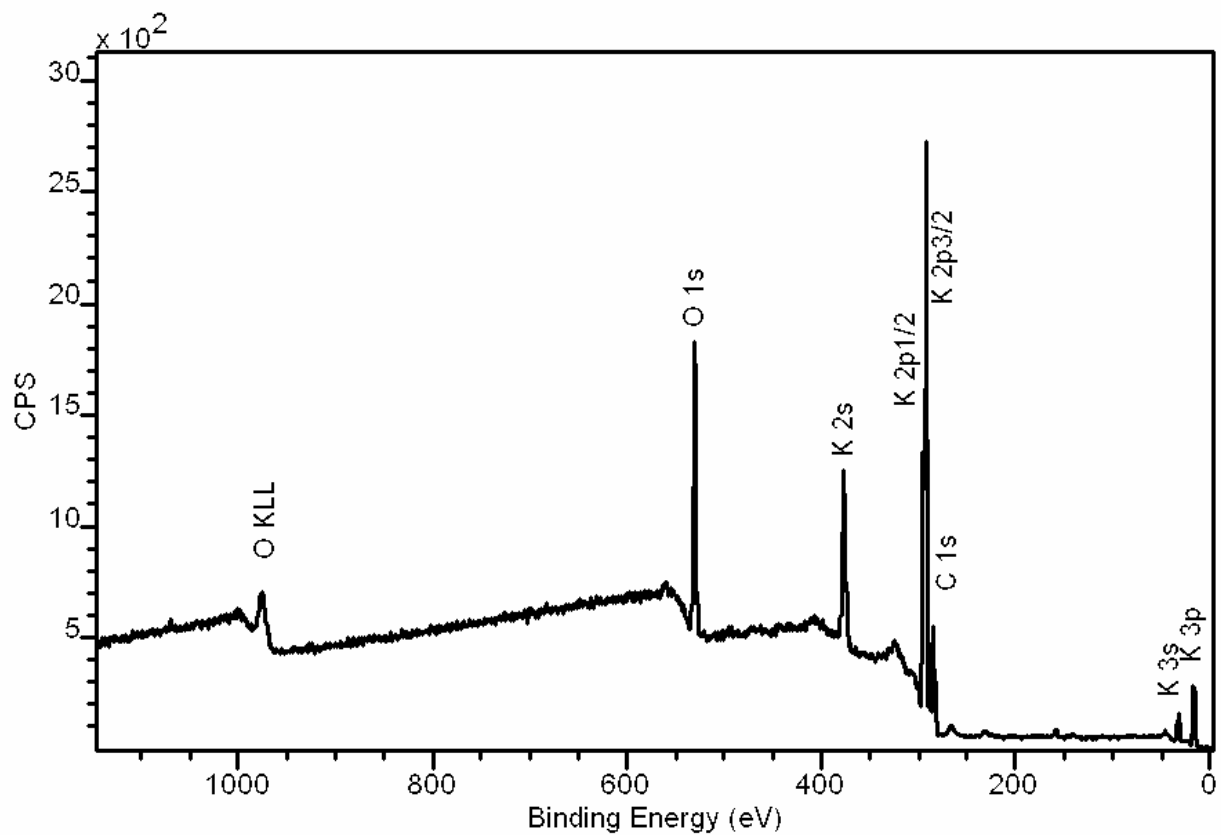


Figure 16. High resolution XPS spectrum ($E_B = 0$ eV to 120 eV) recorded on the reaction product of 8.3g KH + 12g Pd/C that produced an excess energy of 9.94 kJ having peaks at 8.9 eV and 10.7 eV that could not be assigned to known elements and do not correspond to any other primary element peak but do match the $H^- (1/4) E_b = 11.2$ eV hydride ion in two chemical environments.

